

## Chapter 3

### **Geochronology and geochemistry of Iranian Paleogene volcanism: an extensional arc flare-up**

#### **ABSTRACT**

New U-Pb and  $^{40}\text{Ar}/^{39}\text{Ar}$  geochronology demonstrate that shallow marine to continental volcanism within the Iranian Urumieh-Dokhtar arc was dominated by an Eocene pulse, ~20 My in duration, that is not readily explainable by changes in the subduction rate of Neotethyan oceanic crust. Tertiary submarine volcanic and volcanoclastic deposits in the Alborz Mountains of northern Iran as well as volcanic rocks in the Lut block of eastern Iran are also primarily Eocene in age. Eocene volcanism was enriched in large ion lithophile elements (LILE) and depleted in high-field strength elements (HFSE), a pattern typical of arc magmatism. In contrast, Oligocene basalts from the Urumieh-Dokhtar arc and the Alborz Mtns. are enriched in both LILE and HFSE, features consistent with the generation of magmas from undepleted, asthenospheric mantle. Zr/Nb and Ti/V ratios suggest that the Oligocene basalts were derived from a relatively unoxidized mantle source that is unexpected in volcanic arcs. Together with the recent recognition of Eocene metamorphic core complexes in central and east-central Iran and stratigraphic evidence for Eocene subsidence, these geochemical and geochronological data suggest that the magmatic pulse was related to extension, in contrast to compression-driven flare-ups in the western North American batholith and the Andean volcanic arc. Geochemical, geochronological, and stratigraphic data from the Iranian arc are consistent with an Eocene magmatic pulse that was generated by decompression melting of hydrated, slab-fluid modified lithospheric mantle in the mantle wedge, followed by Oligocene upwelling

and melting of asthenospheric mantle that was less extensively modified by hydrous fluids. Slab-rollback, facilitated by the particularly slow Arabia-Eurasia convergence rate and possibly preceded by a Cretaceous period of flat-slab subduction, may have initiated extension and ignited the flare-up. Neogene volcanism in the eastern Mediterranean region and along the western Trans Mexican Volcanic belt may be well-characterized, recent analogs for the Iranian Eocene flare-up.

## **INTRODUCTION**

Flux-melting models of arc volcanism predict that magma production is closely related to the supply of slab-derived hydrous fluids (e.g., Gill, 1981, McCulloch and Gamble, 1991, Davies and Stevenson, 1992). Regardless of whether these fluids originate from subducted sediments (e.g., Plank and Langmuir, 1993) or hydrous melts of oceanic crust (e.g., Elliott, 2003), the rate at which they are replenished is closely tied to subduction rate (e.g., Davies and Bickle, 1991). Although subduction rate and volcanic output are correlated in some cases (Huang and Lundstrom, 2007), it has become increasingly clear that magmatic production in some arcs is distinctly episodic and that the “flare-ups” responsible for the actual creation of these arcs are not related to changes in subduction rate (Ducea, 2001; Ducea and Barton, 2007). These observations suggest that conventional flux-melting models do not fully account for magma generation processes that operate at some convergent margins. One of these processes may be mantle upwelling, which is linked with volcanism in back-arc basins (e.g., Gribble et al., 1998) and may generate melting beneath volcanic fronts as well (e.g., Sisson and Bronto, 1998).

Two notable examples of magmatic flare-ups are 1) the Cretaceous arc of western North America, where despite a >100 My history of subduction, the batholith is dominated by two pulses, each lasting only 10-15 My (Ducea, 2001); and 2) episodic Miocene to Recent mafic volcanism in the Andean Puna Plateau (e.g., Kay et al., 2005). In both of these examples geologic evidence of syn-magmatic compression has led to models that link flare-ups to shortening of the overriding tectonic plate. In the model of Kay and Kay (1993), shortening and thickening increase the density of the base of the crust, eventually leading to delamination of the lower crust and lithospheric mantle. Partial melting of rising asthenospheric mantle subsequently generates a volcanic pulse. Ducea and Barton (2007) presented isotopic evidence that the North American arcs were derived from the crust and therefore proposed that flare-ups can occur when thickening leads to melting of the lower crust.

In this paper we address one of the most impressive yet understudied magmatic flare-ups in earth history, the Paleogene volcanism in Iran. Mixed volcanic and sedimentary sequences of this age in both the Urumieh-Dokhtar arc in central Iran and the Alborz Mountains in northern Iran are ~3-9 km thick (Figure 1, e.g., Förster et al., 1972, Hassanzadeh, 1993). Marine fossil assemblages within these strata are indicative of a pulse of Eocene submarine volcanism (e.g., Berberian and King, 1981) related to the slow (~3 cm/yr) subduction of Neotethys beneath Iran (McQuarrie et al., 2003). Mesozoic igneous rocks are virtually non-existent within both ranges despite a history of subduction that probably began in late Triassic time, as discussed below. Proposed explanations for the Eocene flare-up have included rifting/back-arc basin development

(Amidi et al., 1984, Amidi and Michel, 1985, Kazmin et al., 1986), changes in subduction angle (Berberian and Berberian, 1981, Shahabpour, 2007), and changes in subduction rate (Takin, 1972, Pazirandeh, 1973, Kazmin et al., 1986). Many previous geochemical studies of Iranian volcanism have been hindered by a lack of stratigraphic context or geochronological data and have not fully addressed complicating issues such as crustal assimilation and secondary alteration, leading to a regional dataset of major and trace element analyses that is difficult to interpret in terms of mantle processes.

In order to clarify these issues, we have conducted a study that 1) places U-Pb and  $^{40}\text{Ar}/^{39}\text{Ar}$  age constraints on the duration of the flare-up, and 2) utilizes major and trace element data from primitive mafic rocks erupted during and after the flare-up to identify temporal changes in the source(s) of magmas. Our geochronology data indicate that the magmatic pulse manifested in the Urumieh-Dokhtar arc and the Alborz Mtns. overlaps in time with the formation of Eocene metamorphic core complexes in central and east-central Iran (Moritz et al., 2006, Verdel et al., 2007) and Eocene normal faulting in the Alborz Mtns. (Guest et al., 2006a). Thus, in contrast to the examples from Cordilleran arcs, in Iran there is clear geologic evidence that the flare-up occurred at a time when the overriding plate was being extended. When placed in the context of regional volcanic and sedimentary stratigraphy, new geochemical data from a subset of primitive lavas illustrate a late Eocene-early Oligocene transition from a period of extensive, basaltic to rhyolitic, late Paleocene to Eocene volcanism with typical arc trace element compositions to a later period of limited mafic Oligocene magmatism with trace element compositions similar to those of oceanic island basalts (OIB). We propose that the Eocene flare-up was

generated by decompression melting of preconditioned, hydrated peridotite in the mantle wedge in response to crustal thinning associated with extension. Subsequent Oligocene OIB-type volcanism was produced as upwelling asthenosphere replaced the thinned lithospheric mantle.

We begin by reviewing the Mesozoic and Cenozoic history of Tethyan subduction and the Tertiary stratigraphic record of volcanism and basin formation within Iran. We then present U-Pb,  $^{40}\text{Ar}/^{39}\text{Ar}$ , and major and trace element data from Tertiary volcanic rocks in the Urumieh-Dokhtar arc and the Alborz Mountains. Finally, we propose a mechanism for generating extension-related magmatic flare-ups that accounts for the geochronological, geochemical, and stratigraphic observations from Iran.

## **REGIONAL GEOLOGY**

Complete discussions of the tectonics and paleogeographic evolution of Iran can be found in Stöcklin (1968), Berberian and King (1981), Dercourt et al. (1986), Ramezani and Tucker (2003), and McQuarrie et al. (2003). Summarized here are the events most pertinent for the generation of arc magmas across central Iran. The various continental blocks that comprise Iran are believed to have been situated along the Paleotethyan margin of Gondwana prior to Permian rifting that separated Iran from Gondwana and opened the Neotethys oceanic basin in its wake (e.g., Ramezani and Tucker, 2003, Hassanzadeh et al., 2008), leaving the Iranian fragments situated between one ocean basin that was expanding and another that was being consumed (Berberian and King, 1981). Neotethys thus widened as Iran was pulled away from Gondwana by the

subduction of Paleotethys beneath the southern margin of Eurasia. A regional unconformity separating rocks as young as Middle Triassic from overlying strata as old as Rhaetic-Liassic is generally interpreted as marking the Middle to Late Triassic closure of Paleotethys (e.g., Stöcklin, 1968, Horton et al., 2008). Plutons of roughly the same age in the Sanandaj-Sirjan zone of southwest Iran (Fig. 1) suggest that subduction of Neotethys beneath Iran initiated at about this time (Berberian and Berberian, 1981, Berberian et al., 1982, Kazmin et al., 1986, Arvin et al., 2007), and may, in fact, have been a direct consequence of the collision between northern Iran and Eurasia (Berberian and King, 1981). Continued subduction and arc magmatism through the Mesozoic is indicated by scattered Jurassic to Cretaceous intrusive rocks within the Sanandaj-Sirjan zone (Fig. 1, Berberian and Berberian, 1981). The distribution of these Mesozoic arc remnants relative to Tertiary volcanic rocks within the Urumieh-Dokhtar arc suggests that the axis of magmatism shifted to the northeast from its initial position within the Sanandaj-Sirjan zone in late Cretaceous or early Tertiary time. On the basis of recent paleogeographic reconstructions (McQuarrie et al., 2003), thermochronometry data from the Alborz Mountains (Axen et al., 2001, Guest et al., 2006b), and new estimates for the age of synorogenic sediments in the Zagros Mtns (Fakhari et al., 2008), Neotethys is believed to have closed from Late Oligocene to Miocene time, initiating the collision between Arabia and Eurasia. Ophiolite outcrops near the Main Zagros reverse fault, which generally separates the Sanandaj-Sirjan zone from the Zagros Mountains (Fig. 1), are believed to mark the suture between Arabia and Eurasia. This interpretation of Iranian regional geology suggests that subduction of Neotethys beneath Iran was on-

going from approximately Late Triassic until at least Late Oligocene time, some 175 million years.

### **ARC STRATIGRAPHY**

Paleogene volcanic rocks crop out in three general regions within Iran (Fig. 1). The first is along a NW-SE belt that extends ~1500 km across the central part of the country. This belt, named the Urumieh-Dokhtar arc in reference to localities at either end, terminates rather abruptly to the southeast near the Pakistan border and merges with volcanic rocks in the Lesser Caucasus and Alborz Mtns. to the northwest. The arc is subparallel to, and approximately 175-200 km northeast of, the Main Zagros reverse fault, although Neogene compression within the Sanandaj-Sirjan zone may have shortened this arc-trench gap since the time of active subduction (Berberian and Berberian, 1981). The Lesser Caucasus/Alborz outcrop belt extends southeast to near Semnan, where it becomes discontinuous and extends into eastern Iran. The third region is a large area of Tertiary volcanic rocks in the Lut block of eastern Iran. Our study is focused on the first two regions. Geochemical studies of volcanism in eastern Iran have been particularly sparse; Jung et al. (1984) is one of the few publications available.

Tertiary volcanic rocks in the Alborz Mtns. and Urumieh-Dokhtar arc unconformably overlie Mesozoic sections generally consisting of marine carbonates and siliciclastic rocks. Although separated by up to several hundred km, the general Tertiary stratigraphy in these ranges is remarkably similar. In both, the older part of the Tertiary section is made up of volcanic rocks of wide-ranging composition interbedded with marine and

continental sedimentary strata. Evidence for submarine volcanism, including pillow lavas, has been widely reported (Stöcklin, 1968, Förster et al., 1972, Alberti et al., 1979, Amidi et al., 1984, Spies et al., 1984, Amidi and Michel, 1985, Hassanzadeh, 1993).

This volcanic and sedimentary part of the section, which makes up the majority of the Tertiary outcrops shown on Fig. 1, is typically overlain, in both arc segments, by the late Eocene-early Oligocene Lower Red Formation, consisting of conglomerate, sandstone, shale, and gypsum, as well as relatively limited pyroclastics and volcanic flows.

Conformably overlying the Lower Red Fm. are ~1200 meters of marine limestones and marls comprising the Oligocene to early Miocene Qom Formation. Mafic lava flows are present within the Qom Formation in the Urumieh-Dokhtar arc and immediately below the Qom-correlative Gand Ab limestones in the western Alborz Mtns., where they have yielded  $^{40}\text{Ar}/^{39}\text{Ar}$  whole rock ages of ~33 Ma (Guest et al., 2007b). The Qom Fm. is conformably overlain by gypsum-bearing red beds of the Miocene Upper Red Formation and continental Pliocene and Quaternary sediments.

The Cenozoic stratigraphic record in the Alborz Mtns and Urumieh-Dokhtar arc, and across much of Iran, thus suggests a Tertiary history that began with a large pulse of shallow marine Eocene magmatism and sedimentation. As volcanism diminished and sea-level fell near the end of the Eocene, gypsum-bearing red beds of the early Oligocene Lower Red Fm. were deposited. Subsidence in the early Oligocene (Guest et al., 2007b) was accompanied by limited basaltic magmatism and led to deposition of the Qom Fm. in central Iran and correlative shallow marine limestones in northern Iran. Deposition of the Miocene Upper Red Formation marks the end of marine conditions over most of Iran.

## GEOCHRONOLOGY

### Urumieh-Dokhtar U-Pb and $^{40}\text{Ar}/^{39}\text{Ar}$ geochronology, Tafresh region

North of the town of Tafresh in central Iran, ~200 km southwest of Tehran, a cross-section through the Urumieh-Dokhtar arc is exposed as the relatively undeformed limb of a northwest-southeast trending syncline. In this area, complexly faulted Mesozoic carbonates and siliciclastic strata are unconformably overlain by the typical arc sequence described above: Paleocene-Eocene volcanic and sedimentary rocks, the Lower Red Fm, carbonates and mafic volcanics of the Qom Fm, and the Upper Red Fm. (Fig. 2). We collected a transect of silicic to intermediate volcanic samples that extends from the base of the volcanic sequence through the Lower Red Formation (Fig. 2). U-Pb zircon ages for the majority of these samples were determined with the UCLA ims1270 ion probe.  $^{40}\text{Ar}/^{39}\text{Ar}$  plagioclase dates were determined at the Nevada Isotope Geochronology Lab.

An andesite flow near the base of the volcanic section has a U-Pb zircon age of  $54.7 \pm 3.1$  Ma ( $2\sigma$ ) (Figs. 2 and 3, Table 1). A sample of green tuff from slightly higher in the section has a plagioclase  $^{40}\text{Ar}/^{39}\text{Ar}$  isochron of  $50.9 \pm 4.4$  Ma and a plateau of  $56.6 \pm 3.9$  Ma (Figs. 2 and 3, Table 2), both of which are statistically indistinguishable from the U-Pb age of the underlying andesite. We consider  $54.7 \pm 3.1$  Ma to be our best estimate for the age of the oldest Tertiary arc volcanism preserved along the transect. Ages decrease up section and reach  $44.3 \pm 2.2$  Ma in the middle of the volcanic section (Fig. 2).

**Karaj Formation U-Pb geochronology, Chalus Road region**

The Eocene Karaj Formation in the Alborz Mtns. of northern Iran is comprised of 3000-4000 meters of volcanic, volcanoclastic, and sedimentary strata that has been subdivided into the following members: lower shale, middle tuff, Asara shale, and upper tuff (e.g., Stöcklin and Setudehnia, 1977). The conspicuously green tuffs and tuffaceous sediments of some renown in Iranian geology are most prevalent within the middle part of this formation, and in some sections within the Alborz Mtns., lavas of dacitic to basaltic composition are present between the Asara shale and the upper tuff member. Samples of tuffaceous material within the Karaj Fm. were collected along the Chalus Road north of Tehran (Figs. 1 and 4). We determined U-Pb ages of  $49.3 \pm 2.9$  Ma for the middle tuff member,  $45.3 \pm 2.3$  Ma for a tuff within the Asara shale, and  $41.1 \pm 1.6$  Ma for the upper tuff member (Figs. 3 and 4).

**Additional U-Pb and  $^{40}\text{Ar}/^{39}\text{Ar}$  geochronology and a composite stratigraphic section**

Building on the extensive geologic mapping performed by the Geological Survey of Iran and previous studies of Iranian Tertiary volcanism, we have assembled a regional volcanic and sedimentary stratigraphy for the Tertiary sections in the Alborz Mtns and Urumieh-Dokhtar arc. In the Alborz Mtns., this regional correlation encompasses geologic maps from the Saveh, Qazvin and Rasht, Tehran, Semnan, and Torud quadrangles (Fig. 5). In each of these areas, Cretaceous rocks, usually limestones, are separated from overlying Tertiary rocks by a prominent unconformity. The oldest Tertiary rocks exposed above the unconformity are conglomerates of the Fajan Formation, or "Eocene basal conglomerate," which are thought to be Paleocene to early Eocene in

age (Stöcklin and Setudehnia, 1977). In the Tehran and Semnan quadrangles, the Fajan Fm is overlain by 400-500 m of marine limestones and marls comprising the Eocene Ziarat Formation. Conformably above the Ziarat Fm. are ~4000 m of sediments and volcanics of the Karaj Formation and equivalent Eocene strata as described above. We determined an additional U-Pb age of  $52.2 \pm 3.4$  Ma for a rhyolitic tuff in the lower part of the Eocene volcanic section ~80 km west of Torud in the eastern Alborz Mtns. (Figs. 1 and 3, Alavi and Hushmandzādeh, 1976). This age is indistinguishable from the oldest Tertiary volcanic ages obtained from both the Tafresh transect in the Urumieh-Dokhtar arc and the Chalus Road transect in the western Alborz Mtns. In addition, we obtained an  $^{40}\text{Ar}/^{39}\text{Ar}$  biotite age of  $37.2 \pm 0.38$  Ma from gabbros that intrude the Karaj Fm near Mobarak-abad, ENE of Tehran. This age is slightly younger than the U-Pb age of  $41.1 \pm 1.6$  Ma determined for the upper tuff member and places a radiometric age constraint on the end of Karaj Fm. deposition. Geochemical data from these late Eocene mafic intrusions are discussed below. Unconformably overlying the Karaj Fm. are sandstones, evaporites, marls, and limestones of the late Eocene Kond Formation which are unconformably overlain by the Oligo-Miocene Lower Red Formation, and the remainder of the section is as described above. The stratigraphic positions of mafic to intermediate samples collected for major and trace element geochemistry and described below are illustrated in Figure 5.

The Tertiary stratigraphy of the Urumieh-Dokhtar arc was compiled in a similar fashion from geologic maps of the Ahar, Saveh, Qom, Aran, Anarak, and Nain geologic quadrangle maps and several studies focused on Tertiary magmatism within the arc (Fig.

6). As noted above, the Tertiary stratigraphy of the Urumieh-Dokhtar arc is essentially the same as in the Alborz Mtns. We determined a U-Pb age of  $37.3 \pm 1.2$  Ma for a welded tuff ~60 km east of Saveh in the northwestern part of the Urumieh-Dokhtar arc (Fig. 3). This age is slightly younger than that determined for the Upper Tuff Member of the Karaj Fm. from the Chalus Road transect but overlaps with the  $^{40}\text{Ar}/^{39}\text{Ar}$  biotite age of gabbros intruding the Karaj Fm. in the Alborz Mtns. We interpret this age as marking the end of the magmatic flare-up. Based on the oldest and youngest U-Pb ages from the main period of volcanism, which are corroborated by  $^{40}\text{Ar}/^{39}\text{Ar}$  ages, we estimate that the magmatic flare-up lasted from  $54.7 \pm 3.1$  Ma (late Paleocene-early Eocene) until  $37.3 \pm 1.2$  Ma (late Eocene), implying a duration of ~13-22 million years. Given the prominent unconformity at the base of the Eocene volcanic section in both the Urumieh-Dokhtar arc and the Alborz Mtns., this is a minimum estimate for the duration of the flare-up.

In general, Mesozoic volcanic strata beneath the Eocene basal conglomerate are thin or absent, although there are exceptions. For instance, up to 1 km of middle to late Cretaceous intermediate to mafic lavas are present in the northern Alborz Mtns. in the Qazvin and Rasht quadrangle (Fig. 1, Annells et al., 1975). In this area the Karaj Fm. reaches a thickness of 6 km, however, suggesting that even in areas where Cretaceous volcanism occurred it was subsidiary to Eocene volcanism and sedimentation. As discussed below, the general distribution of Cretaceous volcanic and intrusive rocks to the northeast of late Triassic and Jurassic plutons (Fig. 1) may imply a Cretaceous period of flat-slab subduction.

Previous radiometric age constraints from the Urumieh-Dokhtar arc as well as our new ages are summarized in Figure 6, as are the stratigraphic positions of samples from the arc that were collected for geochemical investigation. The main pulse of volcanism occurred in the Eocene, but outcrops of younger intrusive and extrusive rocks indicate that magmatic activity continued after the Eocene pulse. This younger phase of magmatism spans from the early Oligocene until Recent time and has been widespread across Iran but volumetrically small compared with the Eocene flare-up. We next discuss geochemical differences that distinguish primitive volcanism erupted during the Eocene and Oligocene periods.

## **GEOCHEMISTRY**

### **Previous work**

Modern, high-quality geochemical investigations of Iranian Tertiary volcanism have been limited compared with many other arcs. We compiled ~275 major element analyses from 10 previous studies focused on the Iranian arcs (see Fig. 1 for the locations of these prior studies). These analyses were compared with large datasets from the Andes and Cascades which typify the basic geochemical attributes of continental arc volcanism. First-order compositional differences between volcanism in Iran and these well-characterized arcs are evident by comparing datasets from each region on total alkali-silica (TAS) diagrams (Figs. 7A, B, C and D). As these diagrams make clear, previous data from Iran suggest that Iranian Tertiary volcanism was significantly more alkaline than arc magmatism in more extensively studied regions. This characteristic of Iranian volcanism has been noted previously (e.g., Amidi et al, 1984, Kazmin et al., 1986, Aftabi

and Atapour, 2000), but has not been fully explained. We discuss the most likely possibilities for the generation of these alkaline lavas later in the paper. A more rigorous analysis of the older Iranian data is difficult because many of the analyses lack trace element, petrographic, and/or stratigraphic information. We discuss below a new suite of samples that, although limited in number, come from key stratigraphic intervals within the Tertiary arcs and capture much of the compositional diversity that has been established by previous studies.

### **Major and trace element data**

Twenty-one new samples of mafic to intermediate lavas and subvolcanic intrusions were collected in the Alborz Mtns., mainly north of Tehran, and in the Urumieh-Dokhtar arc, primarily between the cities of Saveh and Nain (Fig. 1). Mafic samples were preferentially collected in order to minimize the potential effects of differentiation from crustal contamination and fractional crystallization (e.g., DePaolo, 1981). A disadvantage of this approach is that these mafic rocks generally do not contain minerals suitable for U-Pb geochronology. In order to overcome this problem, plagioclase  $^{40}\text{Ar}/^{39}\text{Ar}$  ages were determined for some samples, and relative ages of the remainder were estimated from their stratigraphic position as discussed above.

Major element oxide and trace element (Nb, Zr, Y, Sr, U, Rb, Th, Pb, Ga, Zn, Ni, Cr, V, Ce, Ba, La, and Ti) compositions of these 21 samples were determined using X-ray fluorescence (XRF) at the Ronald B. Gilmore XRF laboratory at the University of Massachusetts (Table 3). Details of the analytical procedure can be found in Rhodes

(1996). The samples range from 44 to 59 wt.% SiO<sub>2</sub>. On a TAS diagram (Fig. 7E), 18 of the 21 samples plot within the field defined by the datasets from the Andes and Cascades, and the remainder (samples TA5, NA3, and TRD5) are unusually alkaline. The alkaline samples, all of which contain the zeolite mineral analcime (NaAlSi<sub>2</sub>O<sub>6</sub>·2H<sub>2</sub>O), would conventionally be called shoshonites. Due to their unusual composition and potential evidence for low-grade metamorphism they are discussed separately below. The 18 remaining “normal” samples can be subdivided into two groups based on the SiO<sub>2</sub> content normally specified as the divide between basalts and andesites: five have >53 wt.% SiO<sub>2</sub>, and 13 have <53 wt.% SiO<sub>2</sub>. Of the basaltic andesite and andesite samples with >53 wt.% SiO<sub>2</sub>, four of them (AN3, DEHNAR1, QM2 and AN5) are classified as medium-K andesites using the scheme proposed by Gill (1981), and the other (AR3) is high-K. Eight of the 13 samples with <53 wt.% SiO<sub>2</sub> are classified as basalts, and the remainder are basanites, trachybasalts, or basaltic trachyandesites. Eight of these mafic samples are alkalic according to the definition of Macdonald and Katsura (1964), three should probably be called “transitional” (Sheth et al., 2002), and the remaining two are sub-alkalic.

The transfer of incompatible elements from subducting slabs to the mantle wedge often results in distinctive trace element compositions of arc volcanism that can be illustrated on normalized trace element diagrams (Fig. 8, e.g., Pearce and Cann, 1973, Gill, 1981). The most common traits of arc volcanism are enrichment, relative to mid-ocean ridge basalts (MORB), of large ion lithophile elements (LILE) such as K, Rb, Sr, Ba, Th, U, and the light rare earth elements (REE), and the relative depletion of high field strength

elements (HFSE) such as Ti, Y, Zr, Nb, and the heavy REE. Enrichment of LILE is generally attributed to the addition of these water-soluble elements by fluids derived from the dehydration of the subducted slab (e.g., Tatsumi et al., 1986), while depletion of the generally fluid-immobile HFSE is thought to reflect a pre-existing depletion within the mantle wedge (e.g., McCulloch and Gamble, 1991, Woodhead et al., 1993, Elliott, 2003). The combination of enrichment in one group of elements and depletion in another results in characteristic “spiked” trace element diagrams. In contrast, back-arc basin basalts (BABB) are normally undepleted in their HFSE compositions (e.g., Woodhead et al., 1993). Because BABB are typically enriched in both LILE and HFSE, they tend to have relatively smooth trace element diagrams. From a practical perspective, trace element compositions of volcanic rocks may not provide any meaningful information about mantle compositions if those rocks did not originate from mantle melts or if extensive differentiation has occurred. This important caveat is discussed at length below, but first we describe the overall major and trace element compositions of our samples.

Trace element data from the five andesitic lavas and intrusions (Fig. 8A) are the most likely to have been affected by assimilation and fractional crystallization, and it is therefore difficult to draw conclusions about mantle compositions from these data. Three of the andesites (AN5, DEHNAR1, and AR3) are Eocene and have strong depletions in Nb, which is probably the most characteristic trace-element feature of arc magmatism (e.g., Gill, 1981). AN3, an Oligocene dike that is the most mafic of the andesite samples, has small positive spikes for the LILE Ba, K, and Sr, possibly related to slab contributions of these elements, but essentially no depletions of the HFSE. QM2, an

Eocene andesite flow from the Urumieh-Dokhtar arc near Tafresh, is Nb depleted and has a positive K spike, typical arc traits, but also contains little La and Ce, which is somewhat unusual because these LREE are fluid mobile and expected to be contributed more extensively by the subducting slab. LREE abundances are often observed to negatively correlate with SiO<sub>2</sub> content, however, so fractional crystallization is a likely explanation for the low LREE concentrations of this lava.

The subalkaline and transitional basalts, all of which are Eocene, have quite uniform trace element compositions (Fig. 8B). These basalts have relative depletions of the HFSE Nb, Zr, Ti, and Y and positive spikes for the LILE Ba, K, and Sr. These characteristics, as well as the general abundance of incompatible elements relative to MORB, can be explained as contributions from a subducting slab and/or assimilation of continental crust, as discussed below. Trace-element diagrams of the eight alkalic basalts (Fig. 8C) are more complicated. Four of these (QM6, SV4, TA1, and TA3) have prominent negative Nb spikes and positive Ba spikes, features consistent with an arc setting. The remaining alkalic basalts lack the characteristic Nb depletion.

As this description makes clear, some samples have all of the trace element characteristics of arc volcanics, e.g., the subalkaline basalts, some have virtually none, e.g., alkaline basalt samples MSHK1 and 7453, and other samples have some of the common characteristics but not all, e.g., QM6 has a negative Nb spike but no positive Sr spike. One complicating factor in evaluating these data is that the samples are of different ages, which has motivated the preceding discussion of geochronology and arc

stratigraphy. Another potential problem inherent to interpreting trace element data from continental arcs is the effect of crustal assimilation (e.g., DePaolo, 1981, Dungan and Davidson, 2004). The trace element composition of bulk continental crust (e.g., Taylor and McLennan, 1985) is quite similar to the composition of typical arc magmas, so extensive assimilation of crustal material can impart an “arc signature” to melts regardless of their original composition. Assuming that assimilation will lead to more silicic compositions, the problem can be minimized to some degree by filtering out all but the most primitive samples. Geochemical criteria modified from Collins (2002) were used to screen out samples that are the most likely to have been affected by crustal contamination and fractional crystallization.

A subset of our samples that meet these criteria ( $<53$  wt.%  $\text{SiO}_2$ ,  $>5$  wt.%  $\text{MgO}$ ,  $>130$  ppm Cr,  $\geq 50$  ppm Ni) are still somewhat removed from mantle compositions, but are nevertheless the most likely to provide insight into mantle compositions (Figs. 8D and E). Sample AN3 has also been included in this group despite containing 53.02 wt.%  $\text{SiO}_2$  because it meets the other geochemical criteria. Three of the basalts within the subset (SV4, TA1 and QZ2; Fig. 8D) contain analcime and will be discussed separately because their original trace element compositions have quite possibly been modified during the formation of analcime (Prelević et al., 2004). Major and trace element data for the remaining primitive and unaltered basalts suggest a key geochemical distinction between the Eocene and Oligocene samples (Fig. 8E). Two Late Eocene subvolcanic mafic intrusions from the Alborz Mtns. have typical arc characteristics, in particular the prominent Nb depletion. Although there are only two Eocene samples in this subset of

primitive basalts, the trace element patterns of all of the Eocene andesites (Fig. 8A) and Eocene shoshonites (Fig. 8F) also have characteristic Nb depletions. In contrast, the four Oligocene samples have quite different trace element compositions, with no Nb depletion and overall flat trace element diagrams. These characteristics are quite similar to OIB (Fig. 8E), but there are some subtle differences. Unlike OIB, sample AR5 has a small positive Sr spike, and three of the four samples have small negative Th spikes. Both of these features are consistent with contributions from slab-derived fluids (Elliott 2003). The fundamental difference between the Eocene and Oligocene samples is that while both groups are enriched in LILE, only the Eocene samples are depleted in HFSE. Both groups display evidence for modification by slab-derived fluids which would suggest continued subduction through the Eocene and early Oligocene.

In addition to trace-element diagrams, ratios of various incompatible elements are often used to infer the tectonic settings of ancient volcanic rocks. In the case of Iranian volcanism, two commonly-used trace element ratios, Zr/Nb and Ti/V, are particularly effective in illustrating the compositional differences between volcanics of different age. Both Zr and Nb are fluid-immobile and resistant to secondary alteration. Because arc lavas are characteristically depleted in Nb, Zr/Nb ratios are typically greater for arc volcanics than MORB or OIB. This ratio can therefore provide some insight into the contributions of subducted slabs in arc and back-arc environments. The basis for tectonic discriminations utilizing Ti and V is the sensitivity of V partitioning to oxygen fugacity ( $fO_2$ ) (Shervais, 1982). Oxidizing environments favor the partitioning of V into melt, whereas Ti partitioning is relatively unaffected by  $fO_2$ . Thus, to first order, oxidizing

conditions will lead to the production of magmas with relatively low Ti/V. MORB, produced under conditions of low  $fO_2$ , typically have Ti/V of 20 to 50, while arc volcanism, generated under more oxidizing conditions, generally has Ti/V of 10 to 20. On plots of Ti/V vs. Zr/Nb, primitive rocks from volcanic arcs would be predicted to have Ti/V of ~10-20 (Shervais, 1982) and Zr/Nb of ~10-100 (Davidson, 1996). In the case of our subset of samples, the two late Eocene intrusions have ratios that are generally in this range (Fig. 9). The Oligocene samples, however, have Zr/Nb ratios of ~3 to 9, and Ti/V ratios of 41 to 56. These values are unusual in arc settings and suggest that the source of the Oligocene volcanism was relatively undepleted in HFSE and unoxidized compared with the Eocene mantle source.

We conclude from this dataset that major and trace element compositions of several Oligocene Iranian basalts contrast with the typical compositions of lavas erupted during the Eocene main phase of volcanism in two fundamental ways. First, the Oligocene magmatism appears to be more mafic overall. These lavas are often primitive basalts, whereas Eocene volcanism was of wide-ranging composition but seldom included primitive mafic lavas. Second, the Oligocene basalts exhibit fewer of the classic geochemical traits of arc volcanism, i.e., Nb and Zr depletions, distinct positive Sr spikes, high Zr/Nb and low Ti/V ratios, which are usually found during the older phase of volcanism. Assuming that the compositions of these basalts are, in fact, related to the trace element compositions of their source, the difference in trace element compositions suggests that the source of magmatism changed in the early Oligocene. The timing of this transition is fairly well-constrained by geochronology data, although it is quite

conceivable that the change was not synchronous over a large area. Sample 7453, an Oligocene basalt flow at the base of the Gand Ab limestones in the Alborz Mtns., has OIB-type trace element characteristics (Fig. 8E) and is stratigraphically equivalent to a basalt dated by  $^{40}\text{Ar}/^{39}\text{Ar}$  whole rock at  $32.7 \pm 0.3$  Ma (Guest et al., 2007b). Comparison of this date with the  $^{40}\text{Ar}/^{39}\text{Ar}$  biotite age of  $37.2 \pm 0.38$  Ma from the Mobarak-abad gabbro, equivalent in age to samples DV1 and DV4 which have typical arc trace element compositions (Fig. 8E), suggests that the transition in magma sources occurred between  $\sim 37$  and 33 Ma. In terms of field relationships, the later period of OIB-type magmatism often occurs as basalt flows just below and within the Qom Fm. and mafic subvolcanic intrusions into the Karaj Formation and equivalent Eocene strata. However, some of the intrusions into the Karaj Fm., such as those represented by samples DV1 and DV4, seem to be slightly older and are part of the earlier period of magmatism with typical arc characteristics. Although additional fieldwork is required in order to fully establish the cross-cutting relationships between these intrusions and overlying formations, the late Eocene-early Oligocene Lower Red Fm. seems to be the key marker bed that separates underlying volcanic rocks with typical arc trace element compositions from overlying OIB-type volcanism. These stratigraphic relationships and a summary of our geochronology and geochemical data are illustrated in Figure 10.

### **Iranian shoshonites**

Shoshonites are high-K volcanic rocks with the following major and trace element characteristics from Morrison (1980): near silica saturated,  $\text{Na}_2\text{O} + \text{K}_2\text{O} > 5$  wt.%,  $\text{K}_2\text{O}/\text{Na}_2\text{O} > 0.5$  at 50 wt.%  $\text{SiO}_2$ , and  $> 1$  at 55 wt.%  $\text{SiO}_2$ ;  $\text{TiO}_2 < 1.3$  wt.%,  $\text{Al}_2\text{O}_3 > 14$

wt.%, low Fe enrichment, and high LILE. Shoshonites of Tertiary age have been widely described in Iran (e.g., Alberti et al., 1979, Amidi et al., 1984, Kazmin et al., 1986, Aftabi and Atapour, 2000). Three of our new samples (TRD5, NA3, and TA5) meet the preceding definition and form an outlying group on a TAS diagram (Fig. 7E). These samples all contain analcime, and previous descriptions of Iranian shoshonites usually mention the presence of analcime (Alberti et al., 1979, Amidi et al., 1984, Hassanzadeh, 1993, Aftabi and Atapour, 2000). As discussed above, three samples that are not shoshonites and which meet our geochemical criteria for primitive volcanism also contain analcime. In all of these samples, analcime occurs as small grains within the groundmass, and in the three shoshonitic samples it also occurs as larger crystals that superficially appear to be phenocrysts (Fig. 11). The widespread occurrence of analcime in Iranian arc rocks, and in particular the close association between analcime and the alkaline rocks that seem to define the first-order compositional difference between the Iranian arc and many other continental arcs (compare Figs. 7B, C, and E), necessitate a closer examination of how analcime formed and its effect on the trace element compositions of the rocks in which it occurs.

Hassanzadeh (1993) and Aftabi and Atapour (2000) suggested that analcime in Tertiary volcanic rocks of the Urumieh-Dokhtar arc formed after leucite ( $\text{KAlSi}_2\text{O}_6$ ). We found no trace of leucite in our analcime-bearing samples using a scanning-electron microscope, although this does not rule out the possibility that it was replaced entirely. Given the lack of clear evidence for a secondary origin, another possibility is that analcime is primary. Debates about the primary or secondary origin of analcime in potassic volcanic rocks

similar to those in Iran have arisen in several locations worldwide (see discussion and references in Prelević et al., 2004). The consensus that has developed in most of these cases is that analcime formed by replacement of a precursor mineral, usually leucite or nepheline, by hydrothermal fluids or during the late stages of crystallization from a hydrous melt (e.g., Karlsson and Clayton, 1991). Although we cannot rule out the primary origin of analcime, descriptions of Tertiary basalts and andesites containing nepheline from the Urumieh-Dokhtar arc (Hassanzadeh, 1993) suggest that the alteration hypothesis is more likely. This explanation, if true, raises doubts about the reliability of geochemical data from analcime-bearing samples because these compositions have almost certainly been modified by reactions with water-rich fluids (Gianetti and Masi, 1989, Prelević et al., 2004). In particular, the scatter displayed by the analcime-bearing samples on the plot of Zr/Nb vs. Ti/V (Fig. 9) may be attributable to changes in the concentration of one or more of these elements during the formation of analcime.

These concerns notwithstanding, analcime-bearing shoshonites are still fairly uncommon rocks, and their presence in Iran may have petrologic and tectonic significance. If the alteration hypothesis is true, it implies that the protoliths of these rocks were highly potassic (Prelević et al., 2004) and contained feldspathoids. The shoshonites analyzed during this study have Rb, Ba, Th, and K concentrations that are 2 to 6 times higher than OIB (Fig. 8F). Potential explanations for enrichment of these elements include addition by hydrous fluids during the formation of analcime, crustal assimilation, extreme additions of fluid-mobile LILE from a subducting slab, derivation from a highly enriched source, and low degrees of partial melting. Additional work is needed to fully understand

the petrogenesis of these lavas, but with the data available it is possible to evaluate the viability of these various options. First, it is important to note that the analcime-bearing primitive basalts have significantly lower LILE concentrations than the shoshonites: the late Eocene to Oligocene basaltic trachyandesite (SV4) has Rb, Ba, Th, and K contents that are only slightly higher than OIB, while the two Eocene basalts (QZ2 and TA1) have less Rb, Th and K than OIB and similar Ba (Fig. 8D). The discrepancy in the concentrations of these elements between the high-K and normal-K samples suggests that the process of forming analcime is not fully responsible for the extreme LILE enrichment and that at least some of this enrichment is a primary feature of the lavas.

While the slightly elevated  $\text{SiO}_2$  content of the shoshonites may indicate some crustal contamination, somewhat specialized and arguably unlikely conditions would be necessary to contribute sufficient LILE through crustal assimilation to match the compositions of the shoshonites while keeping  $\text{SiO}_2$  below 56 wt.%, the highest shoshonite value. For instance, the shoshonites typically contain about twice as much Ba, ~4 times as much K, ~6 times as much Th, and ~10 times as much Rb as the most enriched andesites despite having lower  $\text{SiO}_2$  contents. There is also no obvious correlation between  $\text{SiO}_2$  or MgO and Rb, Ba, Th, or K within the three shoshonite samples. In fact, the shoshonite lava with the highest MgO content (TRD5, 8.02 wt. % MgO) is also the most potassic, ~6 wt. %  $\text{K}_2\text{O}$ .

Large continuous additions of LILE from the subducted slab are unlikely given the slow subduction rate, but pulses of LILE related to slab melting are a possibility, as suggested

by Aftabi and Atapour (2000). The shoshonites analyzed in this study have elevated Sr/Y ratios ( $>40$ ), one of the geochemical traits of adakites, i.e., volcanic rocks thought to be derived from slab melting (Defant and Drummond, 1990). The shoshonites are slightly too mafic to meet the definition of adakite, but Defant and Drummond (1990) note that adakites may be associated with mafic volcanism that is highly enriched in LILE. With the available data, we cannot rule out the possibility that the shoshonites are related to slab melting, nor can we eliminate the possibility that LILE enrichment is due to low degrees of partial melting and/or derivation from an enriched source. These latter two possibilities were proposed by Stern et al. (1988) for the generation of shoshonites with similar LILE enrichments in the Mariana arc, where assimilation of continental crust is a non-factor and secondary enrichment is unlikely. Either explanation is consistent with the Tertiary tectonic setting of Iran: low degrees of partial melting could have been caused by a limited supply of slab fluids resulting from the slow subduction rate, or from mantle upwelling accompanying lithospheric thinning. Alternatively, the subsequent Oligocene OIB-type volcanism suggests that an enriched mantle source may have been available as well.

## **DISCUSSION**

Paleogeographic reconstructions and geologic evidence suggest that Neotethyan oceanic crust was subducted beneath Iran from approximately Late Triassic to Late Oligocene time. Despite this ~175 My history, geochronology data indicate that extensive arc volcanism within the Urumieh-Dokhtar arc and Alborz Mtns. occurred over a period of ~17 My, only 10% of the duration of subduction. Furthermore, volcanic rocks in the arcs

are typically interbedded with sediments containing shallow marine fossil and occasionally display textures suggestive of submarine eruption, i.e., pillows, indicating that shallow marine conditions were maintained despite the accumulation of several km of volcanic and sedimentary rocks. This juxtaposition of continental arc volcanism with marine sedimentation is most readily explained by syn-volcanic subsidence that compensated for the addition of volcanic material during the magmatic flare-up. Eocene extension and associated volcanism and basin formation in Iran have been suggested many times before (Takin, 1972, Pazirandeh, 1973, Amidi et al., 1984, Jung et al., 1984, Amidi and Michel, 1985, Kazmin et al., 1986, Emami, 1991, Hassanzadeh, 1993, Soltani, 2000, Hassanzadeh et al., 2002, Vincent et al., 2005, Guest et al., 2006a and b, Guest et al., 2007b, Shahabpour, 2007) and have recently gained additional support with the recognition of Eocene metamorphic core complexes in central (Moritz et al., 2006) and east-central (Verdel et al., 2007) Iran. Geologic maps and descriptions of the local geology of recently reported eclogite outcrops in the Sanandaj-Sirjan zone near Shahr-e-Kord (Fig. 1, Davoudian et al., 2007) suggest that this area, located in the forearc of Urumieh-Dokhtar, may be another Eocene metamorphic core complex.

### **Mechanism for the Iranian Tertiary flare-up**

Several explanations have been proposed for the Iranian flare-up and shoshonitic volcanism. In this section we evaluate the plausibility of the following mechanisms: change in subduction rate, change in subduction angle, slab melting, and back-arc basin development/rifting. In evaluating these explanations, four key observations must be considered: 1) the Eocene magmatic pulse was largely submarine, 2) Eocene volcanism

occurred ~100 km inland from the remnants of the Mesozoic arc, 3) Oligocene OIB-type mafic magmatism followed the Eocene flare-up, and 4) parts of Iran underwent Eocene extension as indicated by the presence of Eocene metamorphic core complexes.

#### *Changes in subduction rate*

Increased subduction rate would add a proportionally larger supply of hydrous fluids to the subduction zone per unit time, presumably leading to an increase in volcanic activity as predicted by conventional models of flux melting. Kazmin et al. (1986) proposed an explanation analogous to this for the Iranian flare-up while Takin (1972), Pazirandeh (1973), and Hassanzadeh (1993) held the opposite view and argued that subduction slowed in the Eocene because of diminished spreading in the Indian Ocean, leading to extension and volcanism within the Iranian arc. Kinematic reconstructions of Arabia-Eurasia convergence offer a direct means of evaluating these hypotheses. These plate reconstructions show that the rate and obliquity of convergence between Arabia and Eurasia was nearly constant from ~56 to 20 Ma (McQuarrie et al., 2003), signifying that the end of the pulse was not coincident with a change in subduction rate. Longer-term reconstructions by Savostin et al. (1986) suggest that the convergence rate was about 0.7 cm/yr faster during the Eocene than in the Paleocene, lending some support to the notion that the pulse was caused by increased subduction rate. However, considering that many arcs form in settings where convergence rates are ~10 cm/yr (DeMets et al., 1994), it would seem unlikely that an increase of less than 1 cm/yr would generate a sudden magmatic pulse of the magnitude seen in Iran. The Paleogene Arabia-Eurasia convergence rate of ~3 cm/yr is less than half of the present-day Andean convergence

rate (DeMets et al., 1994) and approximately one-third to one-half of the Cretaceous to Jurassic rate between the Farallon and North American plates when nearly all of the plutons in the North American arcs were emplaced (Page and Engebretson, 1984). If first-order comparisons are drawn between the Iranian arc and the Cordilleran arcs of North and South America based on subduction rate, magmatic production should have been relatively limited in Iran, perhaps one half of that in the Cordilleran examples. The limited extent of Mesozoic plutons in the Sanandaj-Sirjan zone suggests that this may, in fact, have been true for the initial axis of the Iranian arc.

#### *Changes in subduction angle*

The Late Cretaceous-early Tertiary inland shift in the locus of arc activity from the Sanandaj-Sirjan zone to the Urumieh-Dokhtar arc (Fig. 1) could be linked to a shallow subduction angle. Berberian and Berberian (1981) and Shahabpour (2007) proposed that various changes in subduction angle could account for the spatial pattern of magmatism within Iran, as well as transitions from compressional to extensional tectonic regimes. In other areas it has been suggested that flat-slab subduction could remove the lithospheric mantle from the overriding plate and trigger upwelling of asthenospheric mantle, potentially explaining the Oligocene OIB-type magmatism. However, this explanation is at odds with the evidence for submarine deposition of the Eocene volcanic and sedimentary strata and the existence of Eocene metamorphic core complexes, both of which suggest a syn-volcanic period of extension and subsidence. Flat-slab subduction is normally associated with contractional deformation and uplift due to increased coupling between the subducting slab and overriding plate, such as in the Laramide orogeny of

western North America (e.g., Bird, 1984). We therefore conclude that it is unlikely that flat-slab subduction was responsible for the key attributes of the Eocene flare-up.

There is some indirect evidence, however, that flat-slab subduction may have occurred during the Cretaceous. First, with the exception of some Cretaceous volcanic rocks in the northwesternmost part of the Sanandaj-Sirjan zone, most Cretaceous magmatism occurred in the northern part of Iran, in contrast to late Triassic to Jurassic plutonism which was concentrated in the southwestern part of the country, i.e., the relict magmatic arc in the Sanandaj-Sirjan zone. Second, a regional unconformity separating Cretaceous sediments from overlying Paleogene volcanic rocks implies a phase of contractional deformation that preceded the Eocene flare-up (e.g., Stöcklin, 1968). This event may correspond with Late Cretaceous to Paleocene cooling of a middle Cretaceous pluton in the Alborz Mtns. (Guest et al., 2006b) and Late Cretaceous folding and thrust faulting in the Sanadaj-Sirjan zone (e.g., Tillman, 1981). We suggest that the apparent Cretaceous shift in magmatism from the Sanandaj-Sirjan zone to northern Iran as well as Late Cretaceous to Paleogene shortening may have resulted from a period of flat-slab subduction that preceded the Eocene flare-up.

#### *Slab melting*

In recent years geochemical evidence has emerged from some arcs which suggests that slab melting may play a role in generating volcanism (e.g., Defant and Drummond, 1990, Gómez-Tuena et al., 2007). The slow convergence rate between Arabia and Eurasia implies that the downgoing slab had a long residence time in the subduction zone which

would have allowed it to heat up and potentially melt. None of the samples analyzed during this study are adakites based on the geochemical criteria specified by Defant and Drummond (1990), but a few samples from Hassanzadeh (1993) do meet these criteria. As discussed above, slab melting may be a viable explanation for generating the extreme LILE enrichment of the Iranian shoshonites. However, aside from the potential for generating volcanism with unusual compositions, slab melting does not explain geologic observations associated with the flare-up such as the inland position of the Tertiary arc or evidence for syn-volcanic subsidence. Furthermore, based on available, albeit limited, geochemical data, Paleogene volcanism with trace element compositions suggestive of slab melting (Defant and Drummond, 1990) seems to be rare in Iran. The absence of data in support of this hypothesis, in conjunction with geologic observations that are not explained by it, lead us to conclude that while slab melting may have occurred, it was not the key process in generating the Eocene flare-up.

#### *Rifting/back-arc basin development*

On the basis of major element data from alkaline Tertiary volcanics, Amidi et al. (1984) and Amidi and Michel (1985) argued that the Urumieh-Dokhtar arc was a linear rift basin unrelated to subduction. While parts of this idea may have some merit as discussed below, the geological and geochemical evidence linking subduction to volcanism within the Iranian arc is overwhelming (e.g., Förster et al., 1972, Takin, 1972, Dewey et al., 1973, Sengör et al., 1993). Kazmin et al. (1986) proposed a related explanation that much of the Eocene volcanism in Iran and throughout the Middle East and Mediterranean was related to back-arc basin development. This mechanism accounts for many of the

characteristics of the Eocene flare-up: the inland position of the Urumieh-Dokhtar arc relative to the Mesozoic arc, syn-extensional volcanism, development of shallow submarine basins, and the BABB geochemical affinity of the Oligocene basalts. However, Eocene volcanism, which was much more voluminous, has trace element compositions that are typical of arcs, not back arcs, and accumulated in many of the same basins as the Oligocene basalts. As an explanation for this discrepancy, we suggest that the mantle source of the Eocene volcanism was metasomatized by slab-derived fluids over the course of ~150 My, from the time of subduction initiation in the late Triassic until the flare-up began in the late Paleocene-early Eocene. Convergence rate was never greater than 3 cm/yr during this period (Savostin et al., 1986), which would have limited the volume of fluids released to the mantle wedge over any given period of time and which may be responsible for the restricted development of the Mesozoic arc. We suggest that this supply of fluids was sufficient to partially hydrate and alter the trace element composition of the mantle wedge but insufficient to induce significant magmatism until extension and decompression melting began. As a result, trace element compositions of Eocene lavas related to decompression but derived from a metasomatized source are indistinguishable from volcanism in other arcs where flux-melting predominates.

### **Conceptual model for the Eocene magmatic flare-up**

Trace element characteristics of Eocene volcanism within the Urumieh-Dokhtar arc, along with the linear trend of the range parallel to the Arabia-Eurasia suture, have led to the predominant view that the belt is a conventional arc analogous to the Andes. We

suggest, alternatively, that the magmatic flare-up was a hybrid of two common end-member mechanisms for generating volcanism: hydration of the mantle wedge by slab fluids as in subduction zones and decompression melting as in mid-ocean ridges (Plank and Langmuir, 1988, Pearce and Parkinson, 1993, Sisson and Bronto, 1998, Conder et al., 2002, Gaetani and Grove, 2003). Geochronology and geochemical data, together with observations of the Iranian Cenozoic stratigraphic record, are consistent with the following two-stage scenario for the Eocene magmatic flare-up and subsequent Oligocene magmatism (Fig. 12).

In the first stage, Eocene extension and crustal thinning, possibly related to slab rollback, generated decompression melting of the sub-arc mantle. Hydrated peridotite in the lithospheric mantle partially melted due to the combined effects of decompression and heating from the underlying upwelling asthenosphere. Both the lithospheric and asthenospheric mantle would have undergone partial melting during this period (Fig. 12). Melting was particularly extensive in the HFSE-depleted lithospheric mantle during this stage because it had been partially hydrated, i.e., preconditioned, during the ~150 My of slow subduction that preceded the flare-up. Melts from the asthenosphere would have been volumetrically small in comparison. Volcanics erupted during this period accumulated in continental and shallow submarine extensional basins, along with abundant sedimentary strata. Slow subduction established the conditions for slab rollback and generated only a limited extent of trench-perpendicular horizontal and downwelling flow within the mantle wedge. Upwelling mantle would therefore have been relatively unencumbered by pre-existing lateral or downward flow. As crustal

thinning progressed, the extent of decompression melting would have increased (Plank and Langmuir, 1988).

Extension directions in the Eocene Golpaygan metamorphic core complex (Moritz et al., 2006) and the suspected Eocene core complex near Shahr-e-Kord (Davoudian et al., 2007) are trench perpendicular. The parallel trends of the Urumieh-Dokhtar extension-related arc, the Mesozoic conventional arc in the Sanandaj-Sirjan zone, and the suture between Arabia and Eurasia also suggest that extension was trench-perpendicular. The most obvious explanation for trench-perpendicular extension is slab rollback (e.g., Lonergan and White, 1997). Rollback and associated extension occur when the subduction rate is large compared to the convergence rate, a condition that has been shown experimentally to be more likely in low convergence rate settings (Schellart, 2005) where coupling and shear stresses between the downgoing slab and overriding plate are relatively small, facilitating extension in the overlying crust (e.g., Jarrard, 1986, Northrup et al., 1995, Gorczyk et al., 2007). Given the evidence for nearly constant, slow Arabia-Eurasia convergence during the Paleogene, it is unclear if extension and resulting volcanism in Iran was triggered by a specific event or was the final result of protracted tension in the overriding plate. As described above, slab rollback may have followed a Cretaceous to Paleocene period of flat-slab subduction, in which case rollback might have accompanied the return to a normal slab dip, as has been suggested for the western U.S. (Humphreys, 1995).

In the second stage, upwelling asthenosphere replaced the thinned lithosphere. Partial melts of the asthenospheric source were responsible for the OIB-like Oligocene magmatism in much the same fashion as widely proposed for generating back-arc basin basalts (e.g., Gribble et al., 1998). Basalts may have been the dominant volcanic lithology during this period because the thinned crust contributed relatively little contamination and was an ineffective density barrier to primitive magmas (Plank and Langmuir, 1988). Trace-element evidence for slab contributions to the Oligocene basalts suggests that subduction was still occurring during this stage. Given the stratigraphic evidence for Oligocene extension, the late Eocene-early Oligocene transition from extensive arc magmatism to limited OIB volcanism probably occurred when the supply of preconditioned mantle wedge was exhausted.

The overall Paleocene to Miocene geologic history thus began with the accumulation of late Paleocene-early Eocene volcanic and sedimentary strata in extensional subsiding submarine basins developed inland of the Mesozoic arc. Deposition continued until at least early Oligocene time, although the continental redbeds of the Lower Red Fm. may mark a latest Eocene to earliest Oligocene hiatus in submarine deposition. The basins were inverted in Late Oligocene or Miocene time (Emami, 2001, Guest et al., 2007a), accompanying the collision of Arabia with Eurasia and are still being uplifted as the collision continues. The best documented example of basin inversion is near Saghand in eastern Iran (Fig. 1, Verdel et al., 2007), where syn-extensional Eocene volcanic and sedimentary strata were deposited in supradetachment basins (see e.g., Friedmann et al., 1994) during core complex formation and were subsequently exhumed by ~N-S

shortening at ~20 Ma (Verdel et al., 2007). Metamorphic core complexes in the Sanandaj-Sirjan zone also have Eocene supradetachment basins (Moritz et al., 2006, Davoudian et al. 2007), although the timing of exhumation is unknown in these areas. These and other outcrops of Eocene volcanic rocks in central Iran are the remnants of small extensional basins, but the two largest in terms of area are the linear basins of Paleogene strata in the Alborz Mtns. and Urumieh-Dokhtar arc. This history of slab rollback, basin formation, OIB-type volcanism, and subsequent basin inversion perhaps represents one cycle in the growth of an extensional-accretionary orogen, according to the definition of Collins (2002). Abundant Eocene and Oligocene volcanism in the Lut block of eastern Iran (Fig. 1) may have developed in a similar tectonic setting as suggested by Jung et al. (1984), although our data do not bear directly on that region.

A similar model for extensional flare-ups was proposed by Lawton and McMillan (1999) for the development of Cenozoic and Mesozoic continental rift magmatism in western North America. There, a remarkably similar transition occurred from an earlier phase of voluminous arc magmatism to a later period of relatively restricted OIB-type volcanism. In the eastern Mediterranean region, it has been argued that an analogous transition was related to extension of the Aegean and Anatolian plates as the result of slab rollback (e.g., Agostini et al., 2007). Wallace and Carmichael (1999), Verma (2002), and Blatter et al. (2007) suggested that decompression melting of asthenospheric mantle was responsible for Neogene extension-related volcanism in the Mexican volcanic belt. In fact, there are several similarities between the Iranian arc and the western part of the central Mexican arc. Subduction of the Rivera plate beneath Mexico has been quite slow (~1-5 cm/yr)

over much of the last 10 million years (DeMets and Traylen, 2000). Some Pliocene-Quaternary lavas from the western part of the Mexican arc were erupted at particularly high rates and have OIB geochemical attributes (Wallace et al., 1992). On a TAS diagram, ~1200 analyses from the Mexican volcanic belt, compiled from the GEOROC database, are scattered toward high alkalinity, similar to Iranian Tertiary volcanism (Fig. 7F). Furthermore, much of the controversy surrounding the primary or secondary nature of analcime has focused on Neogene shoshonites from the Mexican volcanic belt (e.g., Luhr and Kyser, 1989, Karlsson and Clayton, 1991). Not surprisingly, the unusual compositions of these volcanics have prompted a wide range of tectonic and petrologic explanations, including rifting (Verma et al., 2002), slab melting (Gómez-Tuena et al., 2007), interaction with a mantle plume (Márquez et al., 1999), and slab break-off (Ferrari, 2004). However, there seems to be little disagreement that extension played a role in generating volcanism associated with grabens in the western part of the belt (e.g., Wallace et al., 1992).

These similarities suggest that the Mexican volcanic belt and the eastern Mediterranean region may be well-characterized, recent analogs to the Iranian Eocene volcanism. The Iranian case is distinct from these in that the main pulse of Tertiary magmatism in Iran was coeval with extension but had trace element characteristics typical of arcs. OIB type volcanism did not occur until ~15-20 My later. The sheer amount of volcanism and sedimentation accompanying the Iranian example also appears to be a unique characteristic. Extensive preconditioning of the mantle wedge during the ~150 My of subduction preceding the magmatic pulse may be an important factor in the explanation

of both of these differences. Slow subduction rate, coupled with the relatively large consumption of oceanic crust necessary to close the Tethys from Iran's position in the middle to eastern part of Gondwana may have been a unique combination that facilitated extraordinary "preconditioning" and the subsequent Eocene flare-up during rollback.

## **CONCLUSIONS**

We conclude that subduction of Neotethys beneath Iran generated a poorly developed Late-Triassic to Jurassic magmatic arc in the Sanandaj-Sirjan zone. Magmatism seems to have shifted to northern Iran during the Cretaceous, perhaps as the result of flat-slab subduction. Eocene slab rollback extended the overriding plate, creating metamorphic core complexes and rift basins. Large volumes of volcanism were generated for ~20 My during decompression melting of the preconditioned mantle wedge. Subsequent Oligocene basaltic volcanism was sourced from upwelling asthenosphere. Extension ended and the rift basins were inverted when Arabia and Eurasia collided in the Late Oligocene to Miocene.

## **REFERENCES**

- Aftabi, A., and Atapour, H., 2000, Regional aspects of shoshonitic volcanism in Iran: Episodes, v.23, p.119-125.
- Agostini, S., Doglioni, C., Innocenti, F., Manetti, P., Tonarini, S., and Savaşçin, M.Y., 2007, The transition from subduction-related to intraplate Neogene magmatism in the western Anatolia and Aegean area, *in* Beccaluva, L., Bianchini, G., and Wilson, M., eds.,

Cenozoic volcanism in the Mediterranean area: Geological Society of America Special Paper 418, p. 1-15, doi 10.1130/2007.2418(01).

Alavi, M., and Hushmandzādeh, A., 1976, Geological map of the Torud quadrangle: Tehran, Geological Survey of Iran, scale 1:250,000.

Alberti, A., Comin-Chiaramonti, P., Di Battistini, G., Sinigoi, S., and Zerbi, M., 1979, Upper Eocene to early Oligocene shoshonitic volcanism in eastern Azerbaijan: Neues Jahrbuch für Mineralogie (Abhandlungen): v. 134, p. 248-264.

Amidi, S.M., Emami, M.H., and Michel, R., 1984, Alkaline character of Eocene volcanism in the middle part of central Iran and its geodynamic situation: Geologische Rundschau, v. 73, p. 917-932.

Amidi, S.M. and Michel, R., 1985, Cenozoic magmatism of the Surk area (central Iran) stratigraphy, petrography, geochemistry and their geodynamic implications: Geologie Alpine, v.61, p. 1-16.

Anells, R.N., Arthurton, R.S., Bazley, R.A., and Davies, R.G., 1975, Explanatory text of the Qazvin and Rasht quadrangles map: Geological Survey of Iran Geological Quadrangles E3, E4, 94 p.

Arvin, M., Pan, Y., Dargahi, S., Malekizadeh, A., and Babaei, 2007, Petrochemistry of the Siah-Kuh granitoid stock southwest of Kerman, Iran: implications for initiation of Neotethys subduction: *Journal of Asian Earth Sciences*, v. 30, p. 474-489.

Axen, G.J., Lam, P.S., Grove, M., Stockli, D.F., and Hassanzadeh, J., 2001, Exhumation of the west-central Alborz Mountains, Iran, Caspian subsidence, and collision-related tectonics: *Geology*, v. 29, p. 559-562.

Berberian, F., and Berberian, M., 1981, Tectono-plutonic episodes in Iran, *in* Gupta, H.K. and Delany, F.M., eds., *Zagros, Hindu Kush, Himalaya, geodynamic evolution*: Washington, D.C., American Geophysical Union, 323 p.

Berberian, F., Muir, I.D., Pankhurst, R.J., and Berberian, M., 1982, Late Cretaceous and early Miocene Andean-type plutonic activity in northern Makran and central Iran: *Journal of the Geological Society of London*, v. 139, p. 605-614.

Berberian, M., and King, G.C.P., 1981, Towards a paleogeography and tectonic evolution of Iran: *Canadian Journal of Earth Sciences*, v. 18, p. 210-265.

Bird, P., 1984, Laramide crustal thickening event in the Rocky Mountain foreland and Great Plains: *Tectonics*, v. 3, p.741-758.

Blatter, D.L., Farmer, G.L., and Carmichael, I.S.E., 2007, A north-south transect across the central Mexican volcanic belt at  $\sim 100^\circ\text{W}$ : spatial distribution, petrological, geochemical, and isotopic characteristics of Quaternary volcanism: *Journal of Petrology*, v. 48, p. 901-950.

Boccaletti, M., Innocenti, F., Manetti, P., Mazzuoli, R., Motamed, A., Pasquare', G., Radicati di Brozolo, F., and Amin Sobhani, E., 1976, Neogene and Quaternary volcanism of the Bijar area (western Iran): *Bulletin Volcanologique*, v. 40-2, p. 121-132.

Collins, W., 2002, Nature of extensional accretionary orogens: *Tectonics*, v. 21, doi:10.1029/2000TC001272.

Conder, J.A., Wiens, D.A., and Morris, J., 2002, On the decompression melting structure at volcanic arcs and back-arc spreading centers: *Geophysical Research Letters*, v. 29, doi: 10.1029/2002GL015390.

Davidson, J.P., 1996, Deciphering mantle and crustal signatures in subduction zone magmatism, *in* Bebout, G.E., Scholl, D.W., Kirby, S.H., and Platt, J.P., eds., *Subduction top to bottom*, American Geophysical Union, *Geophysical Monograph* 96, 384 p.

Davies, J.H., and Bickle, M.J., 1991, A physical model for the volume and composition of melt produced by hydrous fluxing above subduction zones: *Royal Society of London Philosophical Transactions*, v. 335, p. 355-364.

Davies, J.H., and Stevenson, D.J., 1992, Physical model of source region of subduction zone volcanics: *Journal of Geophysical Research*, v.97, p. 2037-2070

Davoudian, A.R., Genser, J., Dachs, E., and Shabanian, N., 2007, Petrology of eclogites from north of Shahrekord, Sanandaj-Sirjan zone, Iran: *Mineralogy and Petrology*, doi: 10.1007/s00710-007-0204-6.

Defant, M., and Drummond, M., 1990, Derivation of some modern arc magmas by melting of young subducted lithosphere: *Nature*, v. 347, p. 662-665.

DeMets, C., Gordon, R.G., Argus, D.F., and Stein, S., 1994, Effect of recent revisions to the geomagnetic reversal time scale on estimates of current plate motions: *Geophysical Research Letters*, v. 21, p. 2191-2194.

DeMets, C., and Traylen, S., 2000, Motion of the Rivera plate since 10 Ma relative to the Pacific and North American plates and the mantle: *Tectonophysics*, v. 318, p. 119-159.

DePaolo, D.J., 1981, Trace element and isotopic effects of combined wallrock assimilation and fractional crystallization: *Earth and Planetary Science Letters*, v. 53, p. 189-202.

Dercourt, J., Zonenshain, L.P., Ricou, L.E., Kazmin, V.G., Lepichon, X., Knipper, A.L., Grandjacquet, C., Sbertshikov, I.M., Geysant, J., Lepvrier, C., Pechersky, D.H., Boulin, J., Sibuet, J.C., Savostin, L.A., Sorokhtin, O., Westphal, M., Bazhenov, M.L., Lauer, J.P., and Bijuduval, B., 1986, Geological evolution of the Tethys belt from the Atlantic to the Pamirs since the Lias: *Tectonophysics*, v.123, p.241-315.

Dewey, J.F., Pitman, W.C., III, Kyan, W.B.F., and Bonnin, J., 1973, Plate tectonics and the evolution of the Alpine system: *Geological Society of America Bulletin*, v. 84, p.3137-3180.

Ducea, M.N., and Barton, M.D., 2007, Igniting flare-up events in Cordilleran arcs: *Geology*, v.35, p.1047-1050.

Dungan, M.A., and Davidson, J., 2004, Partial assimilative recycling of the mafic plutonic roots of arc volcanoes: an example from the Chilean Andes: *Geology*, v. 32, p. 773-776.

Dupuy, C., and Dostal, J., 1978, Geochemistry of calc-alkaline volcanic rocks from southeastern Iran (Kouh-e-Shahsavaran): *Journal of Volcanology and Geothermal Research*, v. 4, p. 363-373.

Elliott, T., 2003, Tracers of the slab, *in* Eiler, J., ed., *Inside the subduction factory*, American Geophysical Union, *Geophysical Monograph* 138, p. 23-45.

Emami, M.H., 1991, Explanatory text of the Qom quadrangle map, Geological Quadrangle No. E6, Geological Survey of Iran.

Fakhari, M.D., Axen, G.J., Horton, B.K., Hassanzadeh, J., and Amini, A., 2008, Revised age of proximal deposits in the Zagros foreland basin and implications for Cenozoic evolution of the High Zagros: Tectonophysics, doi:10.1016/j.tecto.2007.11.064.

Ferrari, L., 2004, Slab detachment control on mafic volcanic pulse and mantle heterogeneity in central Mexico: *Geology*, v. 32, p. 77-80.

Förster, H., Fesefeldt, K., and Kürsten, M., 1972, Magmatic and orogenic evolution of the central Iranian volcanic belt: 24<sup>th</sup> International Geologic Congress, p.198-210.

Friedmann, S.J., Davis, G.A., Fowler, T.K., Brudos, T., Parke, M., Burbank, D.W., and Burchfiel, B.C., 1994, Stratigraphy and gravity-slide elements of a Miocene supradetachment basin, Shadow Valley, East Mojave Desert, *in* McGill, S.F., and Ross, T.M., eds., Geological investigations of an active margin: Geological Society of America Cordilleran Section guidebook: Redlands, California, San Bernardino County Museum Association, p. 302-318.

Gaetani, G.A., and Grove, T.L., Experimental constraints on melt generation in the mantle wedge, *in* Eiler, J., ed., Inside the subduction factory, American Geophysical Union, Geophysical Monograph 138, p. 107-133.

Ghorbani, M.R., 2006, Lead enrichment in Neotethyan volcanic rocks from Iran: the implications of a descending slab: *Geochemical Journal*, v. 40, p. 557-568.

Gianetti, B., and Masi, U., 1989, Trace-element behavior during weathering of leucite in potassic rocks in potassic rocks from the Roccamonfina volcano (Campania, southern Italy) and environmental implications: *Lithos*, v. 22, p. 317-324.

Gill, J.B., 1981, *Orogenic andesites and plate tectonics*: Springer-Verlag, 390 p.

Gómez-Tuena, A., Langmuir, C.H., Goldstein, S.L., Straub, S.M., and Ortega-Gutiérrez, F., 2007, Geochemical evidence for slab melting in the Trans-Mexican volcanic belt: *Journal of Petrology*, v. 48, p.537-562.

Gorczyk, W., Willner, A.P., Gerya, T.V., Connolly, J.A.D., and Burg, J-P., 2007, Physical controls of magmatic productivity at Pacific-type convergent margins: numerical modeling: *Physics of the Earth and Planetary Interiors*, v. 163, p. 209-232.

Gribble, R.F., Stern, R.J., Newman, S., Bloomer, S.H., and O'Hearn, T., 1998, Chemical and isotopic composition of lavas from the northern Mariana trough: implications for magmagenesis in back-arc basins: *Journal of Petrology*, v. 39, p.125-154.

Guest, B., Axen, G.J., Lam, P.S., and Hassanzadeh, J., 2006a, Late Cenozoic shortening in the west-central Alborz Mountains, northern Iran, by combined conjugate strike-slip and thin-skinned deformation: *Geosphere*, v. 2, p. 35-52.

Guest, B., Stockli, D.F., Grove, M., Axen, G.J., Lam, P.S., and Hassanzadeh, J., 2006b, Thermal histories from the central Alborz Mountains, northern Iran: implications for the spatial and temporal distribution of deformation in northern Iran: *Geological Society of America Bulletin*, v. 118, p. 1507-1521.

Guest, B., Guest, A., and Axen, G., 2007a, Late Tertiary tectonic evolution of northern Iran: a case for simple crustal folding: *Global and Planetary Change*, v. 58, p. 435-453

Guest, B., Horton, B.K., Axen, G.J., Hassanzadeh, J., and McIntosh, W.C., 2007b, Middle to late Cenozoic basin evolution in the western Alborz Mountains: implications for the onset of collisional deformation in northern Iran: *Tectonics*, v. 26,  
doi:10.1029/2006TC002091.

Haghipour, A., and Aghanabati, A., compilers, 1985, Geological map of Iran: Geological Survey of Iran Ministry of Mines and Metals, scale 1:2,500,000.

Haghipour, A., Taraz, H., and Vahdati Daneshmand, F., compilers, 1987, Geological map of the Tehran quadrangle: Geological Survey of Iran, scale 1:250,000.

Hassanzadeh, J., 1993, Metallogenic and tectonomagmatic events in the SE sector of the Cenozoic active continental margin of central Iran (Shahr e Babak area, Kerman Province) [Ph.D. thesis]: Los Angeles, University of California, 204 p.

Hassanzadeh, J., Ghazi, A.M., Axen, G., Guest, B., Stockli, D., and Tucker, P., 2002, Oligocene mafic-alkaline magmatism in north and northwest of Iran: evidence for the separation of the Alborz from the Urumieh-Dokhtar magmatic arc: Geological Society of America Abstract with Programs, v. 34, no. 6, p.331.

Hassanzadeh, J., Stockli, D.F., Horton, B.K., Axen, G.J., Stockli, L.D., Grove, M., Schmitt, A.K., and Walker, J.D., 2008, U-Pb zircon geochronology of late Neoproterozoic-Early Cambrian granitoids in Iran: implications for paleogeography, magmatism, and exhumation history of Iranian basement: Tectonophysics, v.451, p. 71-96.

Hickey, R.L., Frey, F.A., and Gerlach, D.C., 1986, Multiple sources for basaltic arc rocks from the southern volcanic zone of the Andes (34-41°S): trace element and isotopic evidence for contributions from subducted oceanic crust, mantle and continental crust: Journal of Geophysical Research, v. 91, p. 5963-5983.

Horton, B.K., Hassanzadeh, J., Stockli, D.F., Axen, G.J., Gillis, R.J., Guest, B., Amini, A., Fakhari, M.D., Zamanzadeh, S.M., and Grove, M., 2008, Detrital zircon provenance of Neoproterozoic to Cenozoic deposits in Iran: implications for chronostratigraphy and collisional tectonics: *Tectonophysics*, doi: 10.1016/j.tecto.2007.11.063.

Huang, F., and Lundstrom, C.C., 2007,  $^{231}\text{Pa}$  excesses in arc volcanic rocks: constraint on melting rates at convergent margins: *Geology*, v. 35, p.1007-1010.

Humphreys, E.D., 1995, Post-Laramide removal of the Farallon slab, western United States: *Geology*, v.23, p. 987-990.

Jarrard, R.D., 1986, Relations among subduction parameters: *Reviews in Geophysics*, v. 24, p. 217-284.

Jung, D., Keller, J., Khorasani, R., Marcks, C, Baumann, A., and Horn, P., 1984, Petrology of the Tertiary magmatic activity in the northern Lut area, east Iran: *Neues Jahrbuch für Geologie und Paläontologie Abhandlungen*, v. 160, p. 417-467.

Karlsson, H.R., and Clayton, R.N., 1991, Analcime phenocrysts in igneous rocks: primary or secondary?: *American Mineralogist*, v. 76, p. 189-199.

Kay, R.W., and Kay, S.M., 1993, Delamination and delamination magmatism: *Tectonophysics*, v. 219, p. 177-189.

Kay, S.M., Godoy, E., and Kurtz, A., 2005, Episodic arc migration, crustal thickening, subduction erosion, and magmatism in the south-central Andes: *Geological Society of America Bulletin*, v. 117, p.67-88.

Kazmin, V.G., Sbortshikov, I.M., Ricou, L-E., Zonenshain, L.P., Boulin, J., and Knipper, A.L., 1986, Volcanic belts as markers of the Mesozoic-Cenozoic active margin of Eurasia: *Tectonophysics*, v. 123, p. 123-152.

Lawton, T.F., and McMillan, 1999, Arc abandonment as a cause for passive continental rifting: comparison of the Jurassic Mexican Borderland rift and the Cenozoic Rio Grande rift: *Geology*, v. 27, p. 779-782.

Lonergan, L., and White, N., 1997, Origin of the Betic-Rif mountain belt: *Tectonics*, v. 16, p. 504-522.

Macdonald, G.A., and Katsura, T., 1964, Chemical composition of Hawaiian lavas: *Journal of Petrology*, v. 5, p. 82-133.

Márquez, A., Oyarzun, R., Doblas, M., and Verma, S.P., 1999, Alkalic (ocean-island basalt type) and calc-alkalic volcanism in the Mexican volcanic belt: a case for plume-related magmatism and propagating rifting at an active margin?: *Geology*, v. 27, p. 51-54

McCulloch, M.T., and Gamble, J.A., 1991, Geochemical and geodynamical constraints on subduction zone magmatism: *Earth and Planetary Science Letters*, v. 102, p.358-374.

McQuarrie, N., Stock, J.M., Verdel, C., and Wernicke, B.P., 2003, Cenozoic evolution of Neotethys and implications for the causes of plate motions: *Geophysical Research Letters*, v. 30, 2036, doi:10.1029/2003GL017992.

Moritz, R., Ghazban, F., and Singer, B.S., 2006, Eocene gold ore formation at Muteh, Sanandaj-Sirjan tectonic zone, western Iran: a result of late-stage extension and exhumation of metamorphic basement rocks within the Zagros orogen: *Economic Geology*, v. 101, p. 1497-1524.

Morrison, G.W., 1980, Characteristics and tectonic setting of the shoshonite rock association: *Lithos*, v. 13, p. 97-108.

Northrup, C.J., Royden, L.H., and Burchfiel, B.C., 1995, Motion of the Pacific plate relative to Eurasia and its potential relation to Cenozoic extension along the eastern margin of Eurasia: *Geology*, v. 23, p. 719-722.

Page, B.M., and Engebretson, D.C., 1984, Correlation between the geologic record and computed plate motions for central California: *Tectonics*, v. 3, p. 133-155.

Pazirandeh, M, 1973, Distribution of volcanic rocks in Iran and a preliminary discussion of their relationship to tectonics: *Bulletin Volcanologique*, v. 37, p. 573-585.

Pearce, J.A. and Cann, J.R., 1973, Tectonic setting of basic volcanic-rocks determined using trace-element analyses: *Earth and Planetary Science Letters*, v. 19, p. 290-300.

Pearce, J.A., Harris, N.B.W, and Tindle, A.G., 1984, Trace-element discrimination diagrams for the tectonic interpretation of granitic-rocks: *Journal of Petrology*, v. 25, p.956-983.

Pearce, J.A., and Parkinson, I.J., 1993, Trace element models for mantle melting: application to volcanic arc petrogenesis, *in* Prichard, H.M., Alabaster, T., Harris, N.B.W., and Neary, C.R., eds., *Magmatic processes and plate tectonics*, Geological Society Special Publication no.76, p. 373-403.

Plank, T., and Langmuir, C.H., 1988, An evaluation of the global variations in the major element chemistry of arc basalts: *Earth and Planetary Science Letters*, v. 90, p. 349-370.

Pollastro, R.M., Persits, F.M., and Steinshouer, D.W., compilers, 1999, Map showing geology, oil and gas fields, and geologic provinces of Iran: USGS Open-file report 97-470-G, on compact disc.

Prelević, D., Foley, S.F., Cvetković, V., and Romer, R.L., 2004, The analcime problem and its impact on the geochemistry of ultrapotassic rocks from Serbia: *Mineralogical Magazine*, v. 68, p. 633-648.

Ramezani, J., and Tucker, R.D., 2003, The Saghand region, central Iran: U-Pb geochronology, petrogenesis and implications for Gondwana tectonics: *American Journal of Science*, v. 303, p. 622-665.

Rhodes, J.M., 1996, Geochemical stratigraphy of lava flows sampled by the Hawaii Scientific Drilling Project: *Journal of Geophysical Research*, v. 101, p. 11729-11746.

Savostin, L.A., Sibuet, J-C., Zonenshain, L.P., Le Pichon, X., and Roulet, M-J., 1986, Kinematic evolution of the Tethys belt from the Atlantic Ocean to the Pamirs since the Triassic: *Tectonophysics*, v. 123, p. 1-35.

Schellart, W.P., 2005, Influence of the subducting plate velocity on the geometry of the slab and migration of the subduction hinge: *Earth and Planetary Science Letters*, v.231, p.197-219.

Sengör, A.M.C., Cin, A., Rowley, D.B., and Nie, S-Y., 1993, Space-time patterns of magmatism along the Tethysides: a preliminary study: *The Journal of Geology*, v. 101, p. 51-84.

Shahabpour, J., 2007, Island-arc affinity of the central Iranian volcanic belt: *Journal of Asian Earth Sciences*, v. 30, p. 652-665.

Shervais, J.W., 1982, Ti-V plots and the petrogenesis of modern and ophiolitic lavas: *Earth and Planetary Science Letters*, v. 59, p. 101-118.

Sheth, H.C., Torres-Alvarado, I.S., and Verma, S.P., 2002, What is the “calc-alkaline rock series”? : *International Geology Review*, v. 44, p. 686-701.

Sisson, T.W., and Bronto, S., 1998, Evidence for pressure-release melting beneath magmatic arcs from basalt at Galunggung, Indonesia: *Nature*, v. 391, p. 883-886.

Soltani, A., 2000, Geochemistry and geochronology of I-type granitoid rocks in the northeastern Central Iran Plate [Ph.D. thesis]: Australia, University of Wollongong, 300 p.

Spies, O., Lensch, G., and Mihm, A., 1984, Petrology and geochemistry of the post-ophiolitic Tertiary volcanics between Sabzevar and Quchan, NE Iran: *Neues Jahrbuch für Geologie und Palaontologie Abhandlungen*, v. 168, p. 389-408.

Stern, R.J., Bloomer, S.H., Lin, P-N., Ito, E., and Morris, J., 1988, Shoshonitic magmas in nascent arcs: new evidence from submarine volcanoes in the northern Marianas: *Geology*, v. 16, p. 426-430.

Stöcklin, J., 1968, Structural history and tectonics of Iran: a review: *American Association of Petroleum Geologists Bulletin*, v. 52, p. 1229-1258.

Stöcklin, J., and Setudehnia, A., 1977, Stratigraphic lexicon of Iran, Geological Survey of Iran, Report no. 18, second edition, 376 p.

Sun, S.S., and McDonough, W.F., 1989, Chemical and isotopic systematics of oceanic basalts; implications for mantle composition and processes, *in* Saunders, A.D. and Norry, M.J., eds., *Magmatism in the oceanic basins: Geological Society of London Spec. Pub.* 42, p. 313-345

Takin, M., 1972, Iranian geology and continental drift in the Middle East: *Nature*, v. 235, p.147-150.

Taylor, S.R., and McLennan, S.M., 1985, *The continental crust: its composition and evolution, an examination of the geochemical record preserved in sedimentary rocks:* Oxford, Blackwell Scientific Publications, 312 p.

Tillman, J.E., Poosti, A., Rossello, S., and Eckert, A., 1981, Structural evolution of Sanandaj-Sirjan Ranges near Esfahan, Iran: *AAPG Bulletin*, v. 65, p. 674-687.

Verdel, C., Wernicke, B.P., Ramezani, J., Hassanzadeh, J., Renne, P.R., and Spell, T.L., 2007, Geology and thermochronology of Tertiary Cordilleran-style metamorphic core complexes in the Saghand region of central Iran: *Geological Society of America Bulletin*, v. 119, p. 961-977.

Verma, S.P., 2002, Absence of Cocos plate subduction-related basic volcanism in southern Mexico: a unique case on earth?: *Geology*, v. 30, p. 1095-1098.

Vincent, S.J., Allen, M.B., Ismail-Zadeh, A.D., Flecker, R., Foland, K.A., and Simmons, M.D., 2005, Insights from the Talysh of Azerbaijan into the Paleogene evolution of the South Caspian region: *Geological Society of America Bulletin*, v. 117, p. 1513-1533.

Wallace, P., Carmichael, I.S.E, Righter, K., and Becker, T.A., 1992, Volcanism and tectonism in western Mexico: a contrast of style and substance: *Geology*, v. 20, p. 625-628.

Wallace, P.J., and Carmichael, I.S.E., 1999, Quaternary volcanism near the Valley of Mexico: implications for subduction zone magmatism and the effects of crustal thickness variations on primitive magma compositions: *Contributions to Mineralogy and Petrology*, v. 135, p. 291-314.

Woodhead, J.D., Eggins, S.E., and Gamble, J.G., 1993, High field strength and transition element systematics in island arc and back-arc basin basalts: evidence for multi-phase extraction and a depleted mantle wedge: *Earth and Planetary Science Letters*, v. 114, p. 491-504.

**FIGURE CAPTIONS**

**Figure 1.** Map of Iran highlighting Cenozoic and Mesozoic igneous rocks (modified from Haghypour and Aghanabati, 1985 and Pollastro et al., 1999). Eocene metamorphic core complexes from Moritz et al., 2006, Davoudian et al., 2007, and Verdel et al., 2007. Previous geochemical studies: A-Alberti et al., 1979, B-Boccaletti et al., 1976, C-Ghorbani, 2006, D-Amidi et al., 1984, E-Amidi and Michel, 1985, F-Förster et al., 1972, G-Hassanzadeh, 1993, H-Spies et al., 1984, I-Jung et al., 1984, J-Dupuy and Dostal, 1978.

**Figure 2.** Composite stratigraphy of Cretaceous through Miocene volcanic and sedimentary rocks in the Tafresh area showing geochronology sample locations (modified from Emami, 1991).

**Figure 3.** U-Pb concordia and Tera-Wasserburg plots and  $^{40}\text{Ar}/^{39}\text{Ar}$  spectra and isochrons for volcanic rocks from the Alborz Mtns. and Urumieh-Dokhtar arc.  $^{40}\text{Ar}/^{39}\text{Ar}$  data are from plagioclase; all errors are  $2\sigma$ .

**Figure 4.** Cretaceous through Miocene stratigraphy of the Chalus Road area showing geochronology results (modified from Haghypour et al., 1987).

**Figure 5.** Generalized Tertiary stratigraphy of the Alborz Mtns. showing positions of geochronology and geochemistry samples. Shaded region indicates time of Eocene magmatic flare-up.

**Figure 6.** Generalized Tertiary stratigraphy of the Urumieh-Dokhtar arc showing positions of geochronology and geochemistry samples. Shaded region indicates time of Eocene magmatic flare-up.

**Figure 7.** Total alkali-silica diagrams. (A) Nomenclature. (B) Data from ~1500 Andean samples and ~1000 Cascades samples, compiled from the GEOROC database. (C) Data from ~275 Iranian Tertiary samples, compiled from various sources. (D) Same data as (C) coded by age. (E) 21 new Iranian Tertiary samples, oval drawn around shoshonitic samples. (F) ~1100 samples from the Mexican volcanic belt, compiled from the GEOROC database.

**Figure 8.** Primitive mantle normalized trace element diagrams. (A) Andesites. (B) Subalkaline and transitional basalts. (C) Alkaline basalts. (D) Primitive basalts with analcime. (E) Primitive basalts without analcime. (F) Shoshonites. Primitive mantle, N-MORB and OIB values from Sun and McDonough, 1989. Volcanic arc basalt (VAB) values from Hickey et al., 1986.

**Figure 9.** Ti/V vs. Zr/Nb plot for primitive Iranian basalts.

**Figure 10.** Generalized Tertiary stratigraphy of Iran with radiometric age constraints.

**Figure 11.** Iranian shoshonite sample NA3.

**Figure 12.** Diagram summarizing development of the Eocene arc flare-up and subsequent OIB-type Oligocene magmatism. The continental lithosphere is area-balanced in these schematic cross-sections and is held constant at 100 km thickness at the right edge of the diagram. Abbreviations: UD-Urumieh-Dokhtar magmatic arc, AB-Alborz Mtns, CI-Central Iranian Eocene volcanics between Urumieh-Dokhtar and the Alborz Mtns.

Figure 1

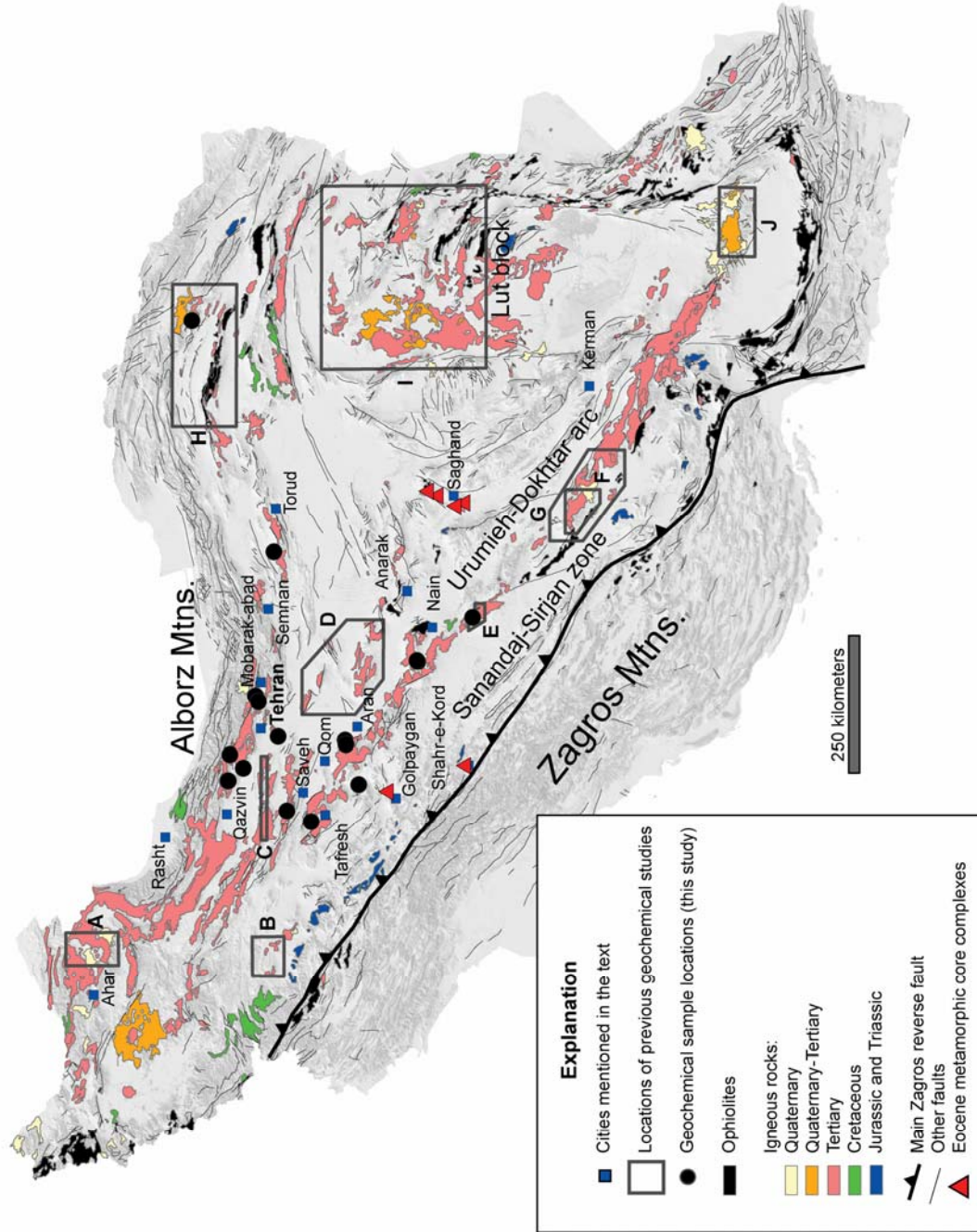


Figure 2

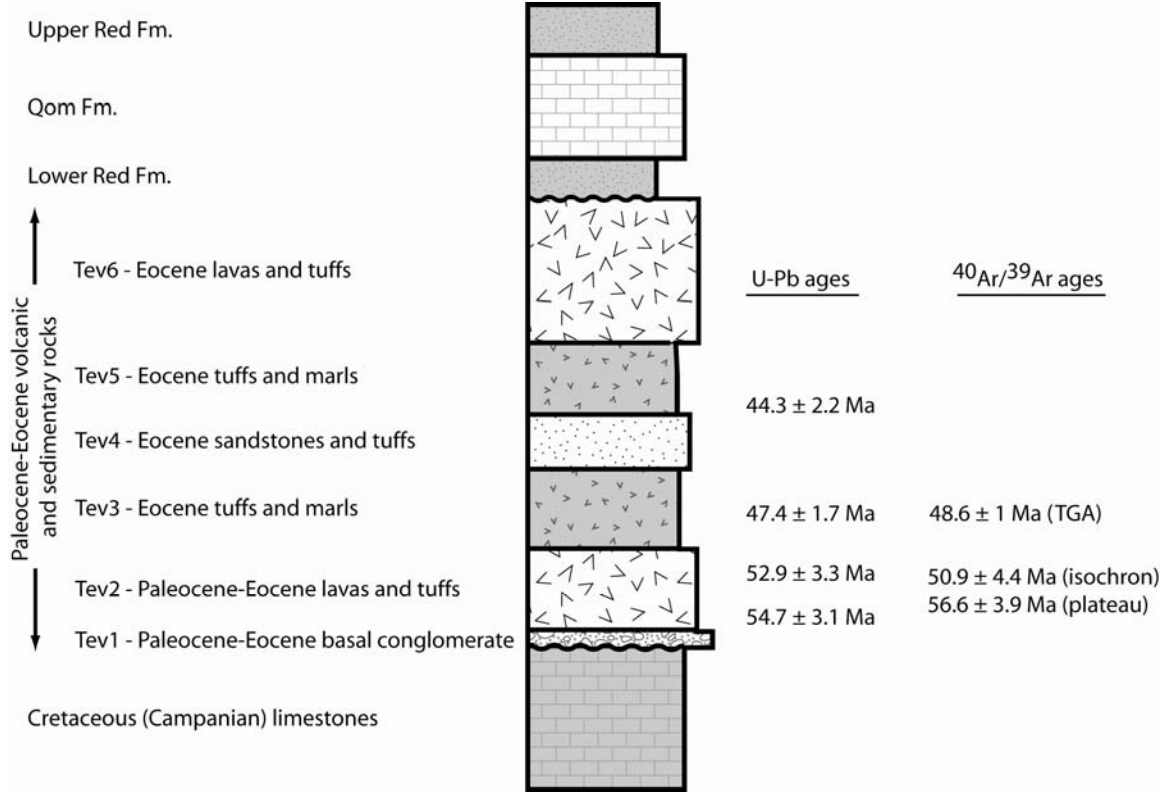


Figure 3

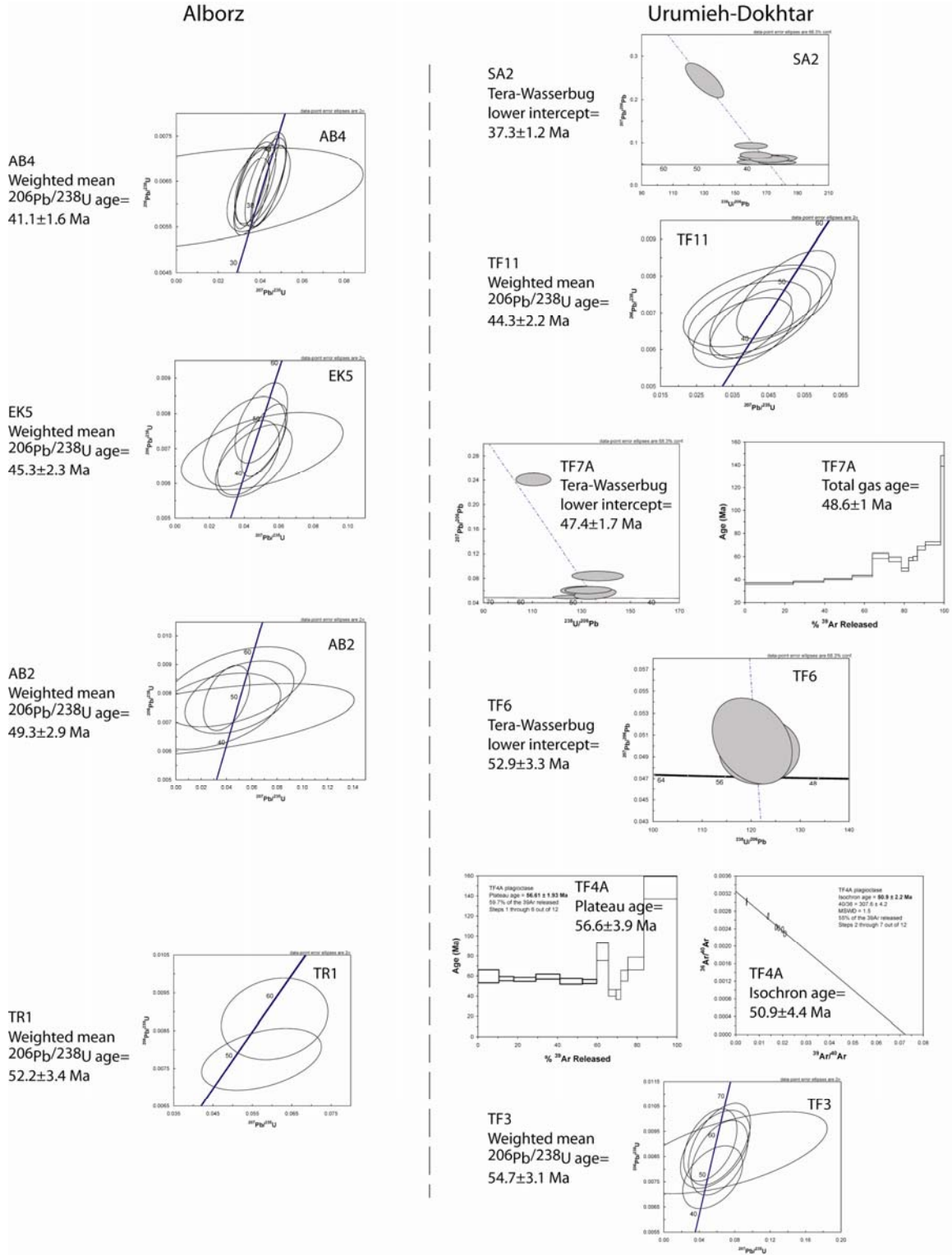


Figure 4

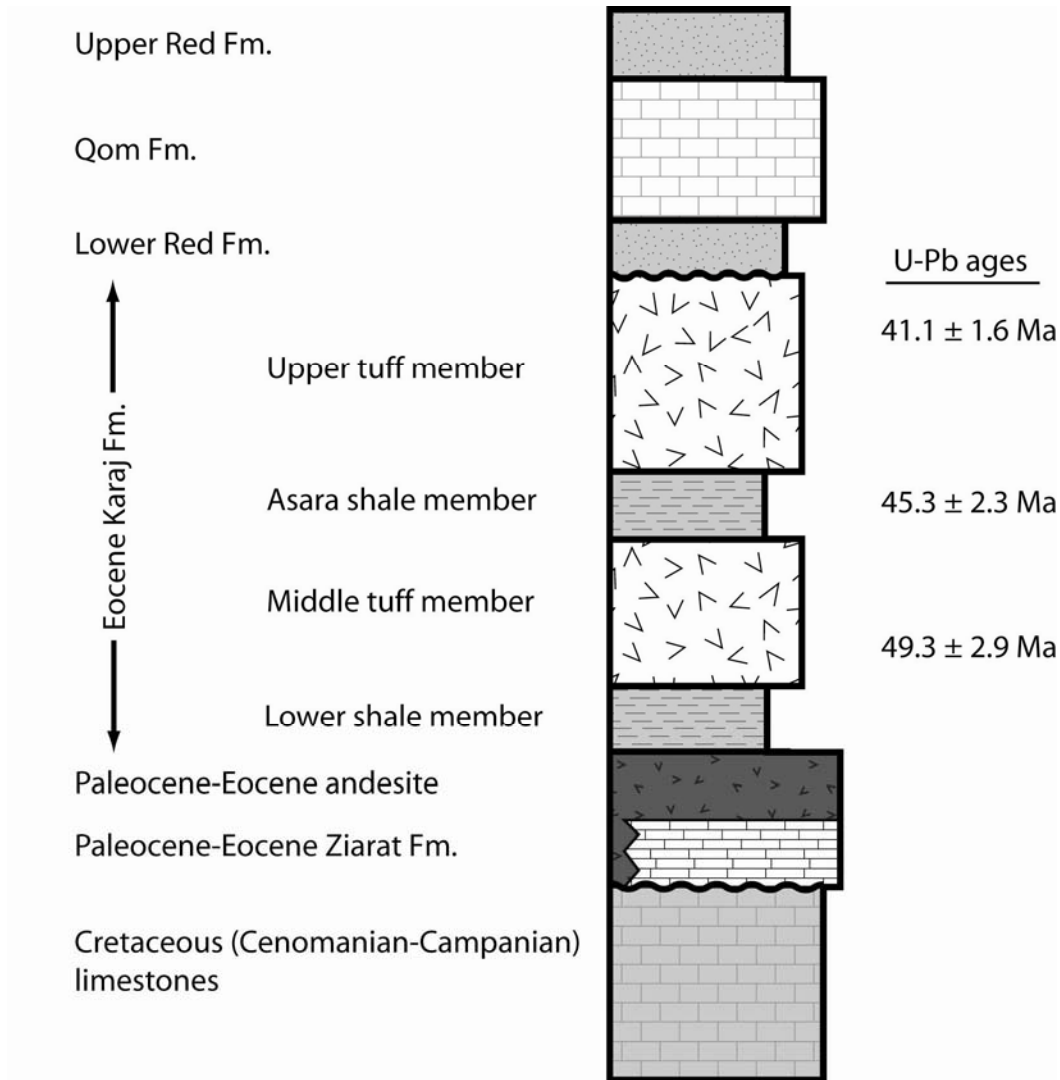


Figure 5

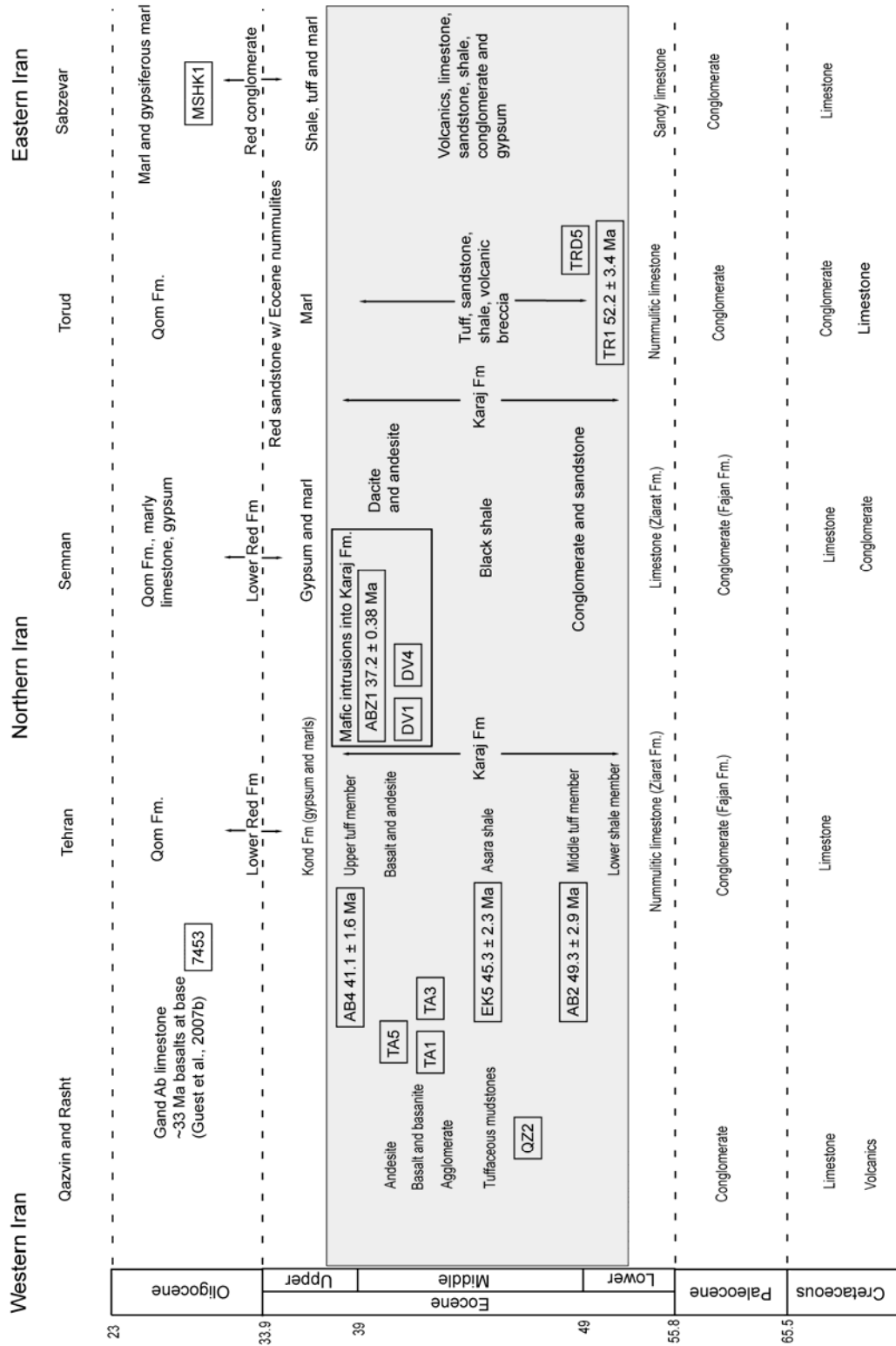


Figure 6

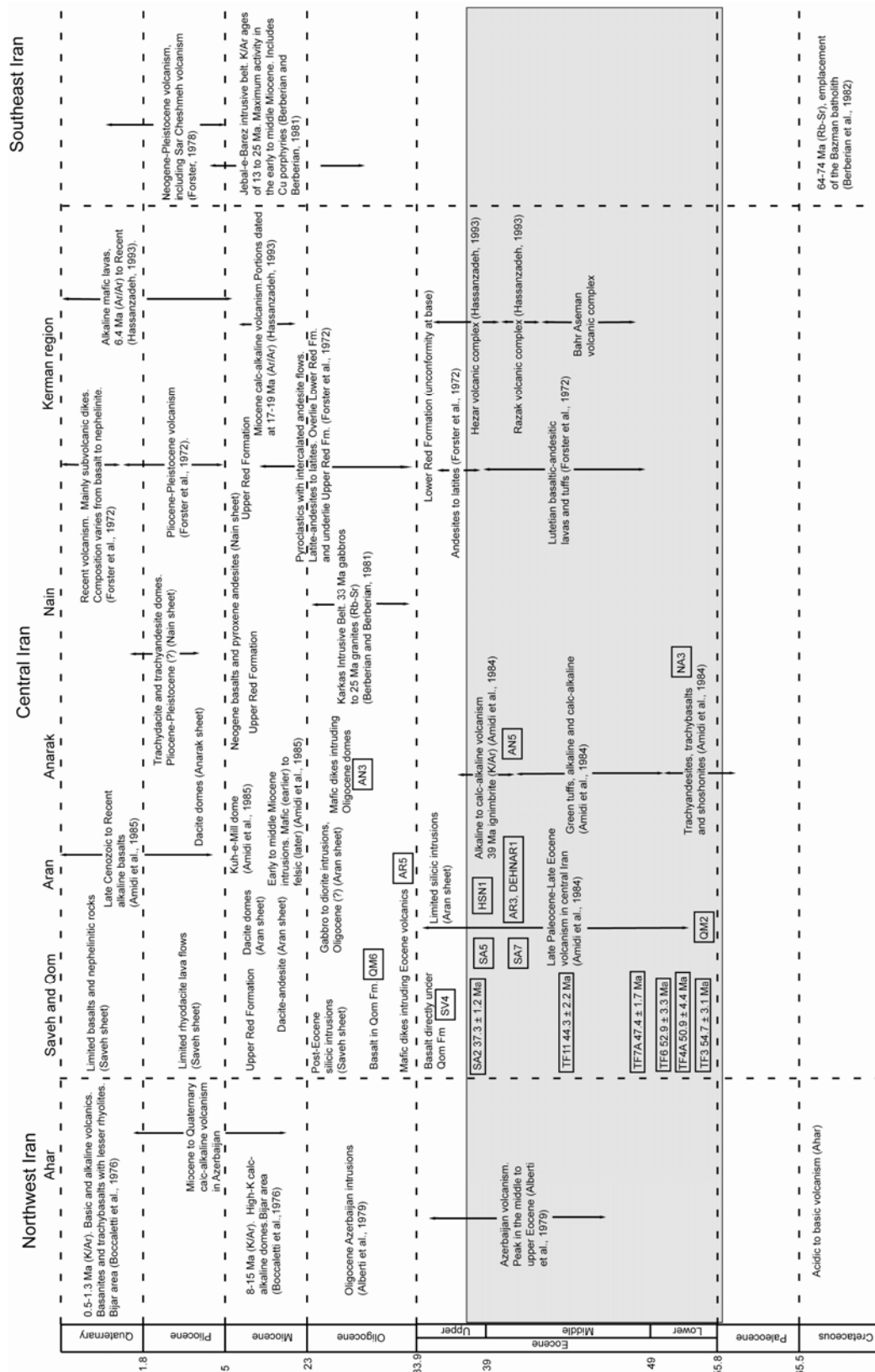


Figure 7

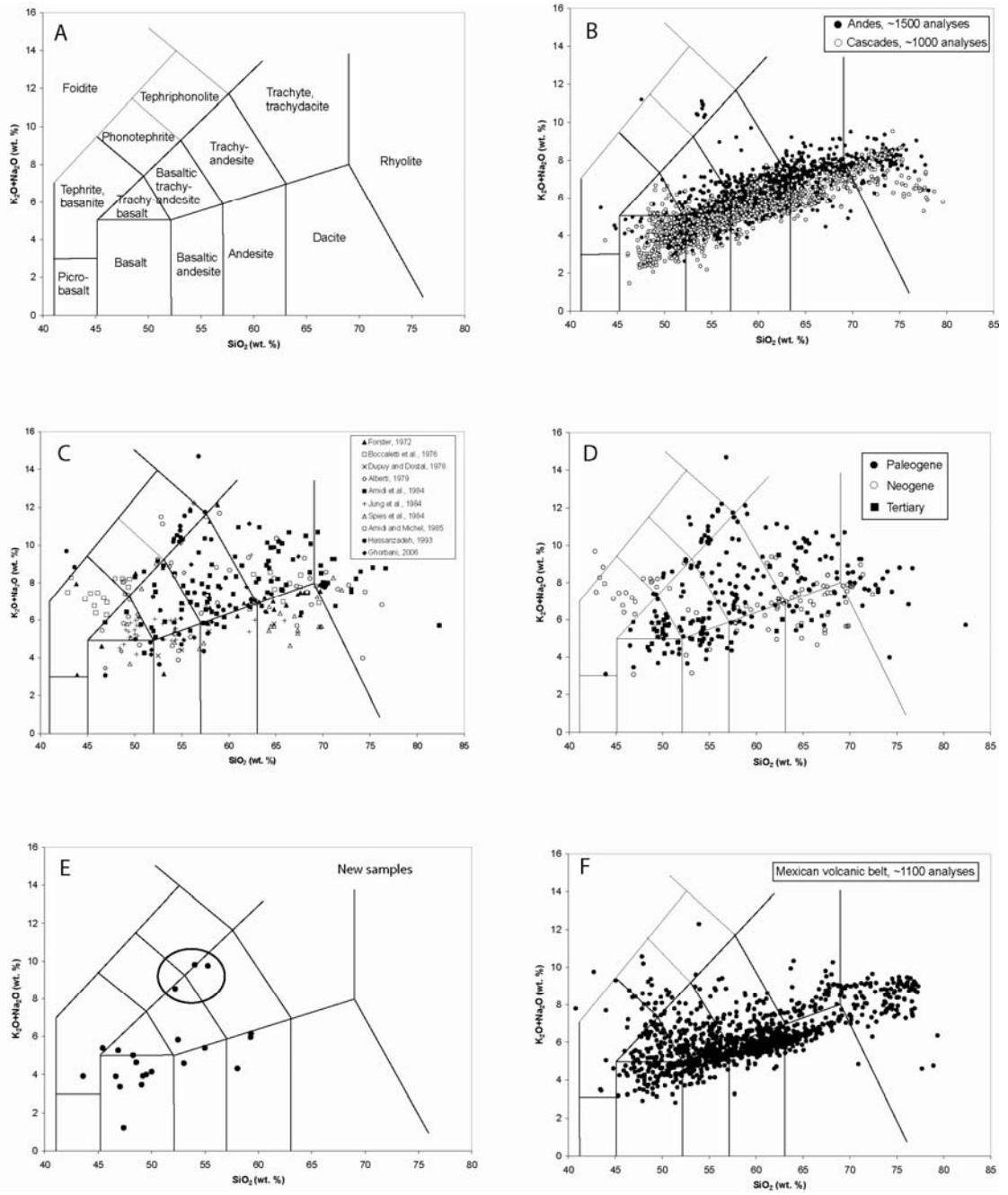


Figure 8

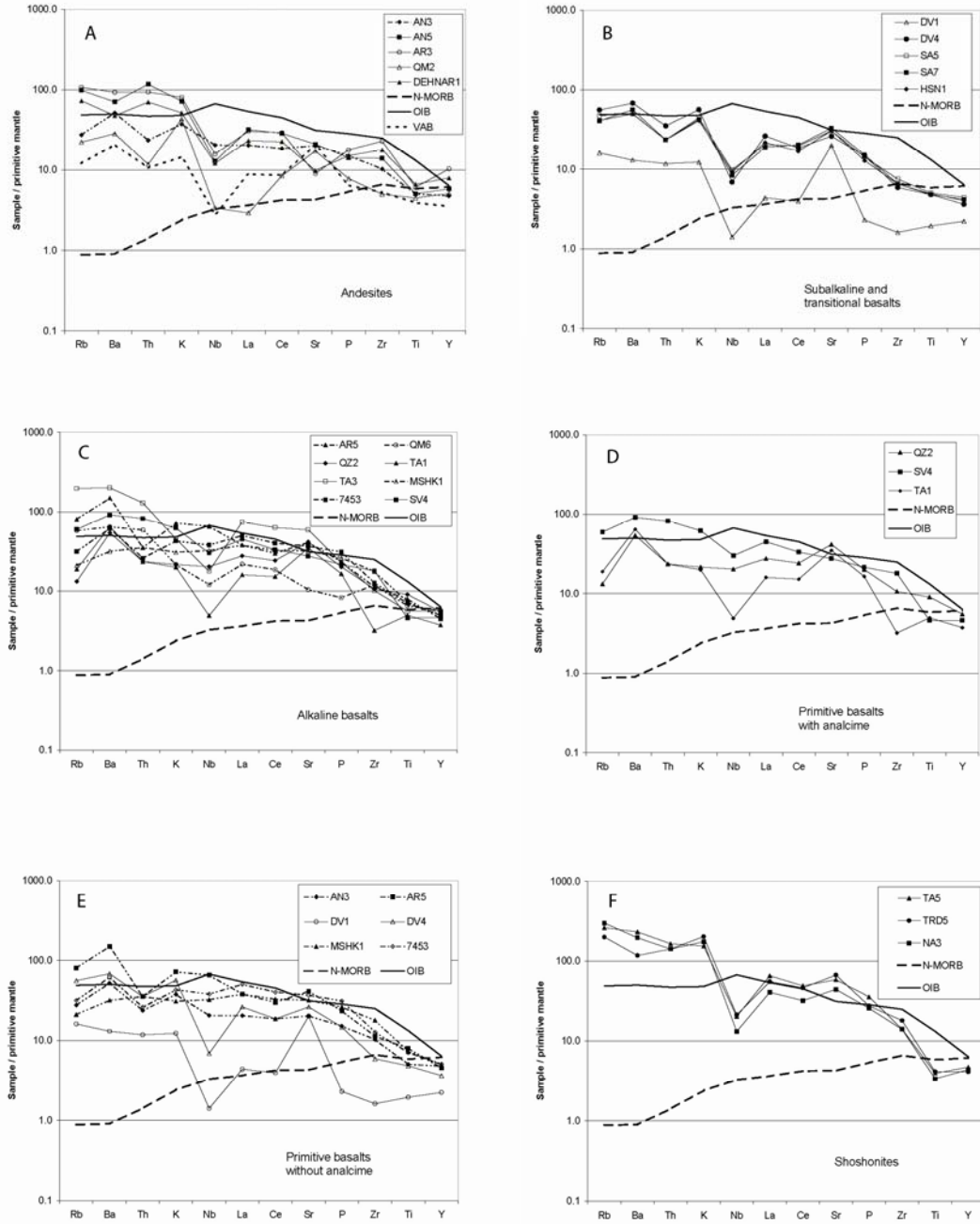


Figure 9

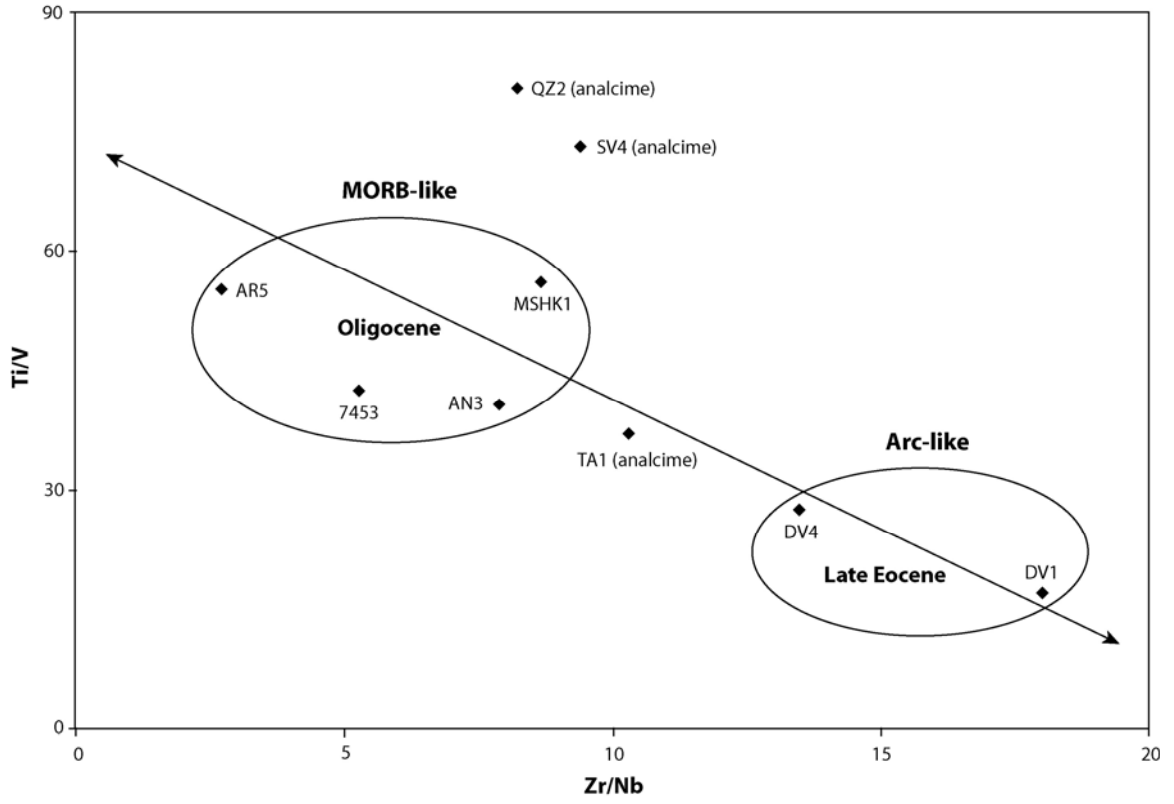
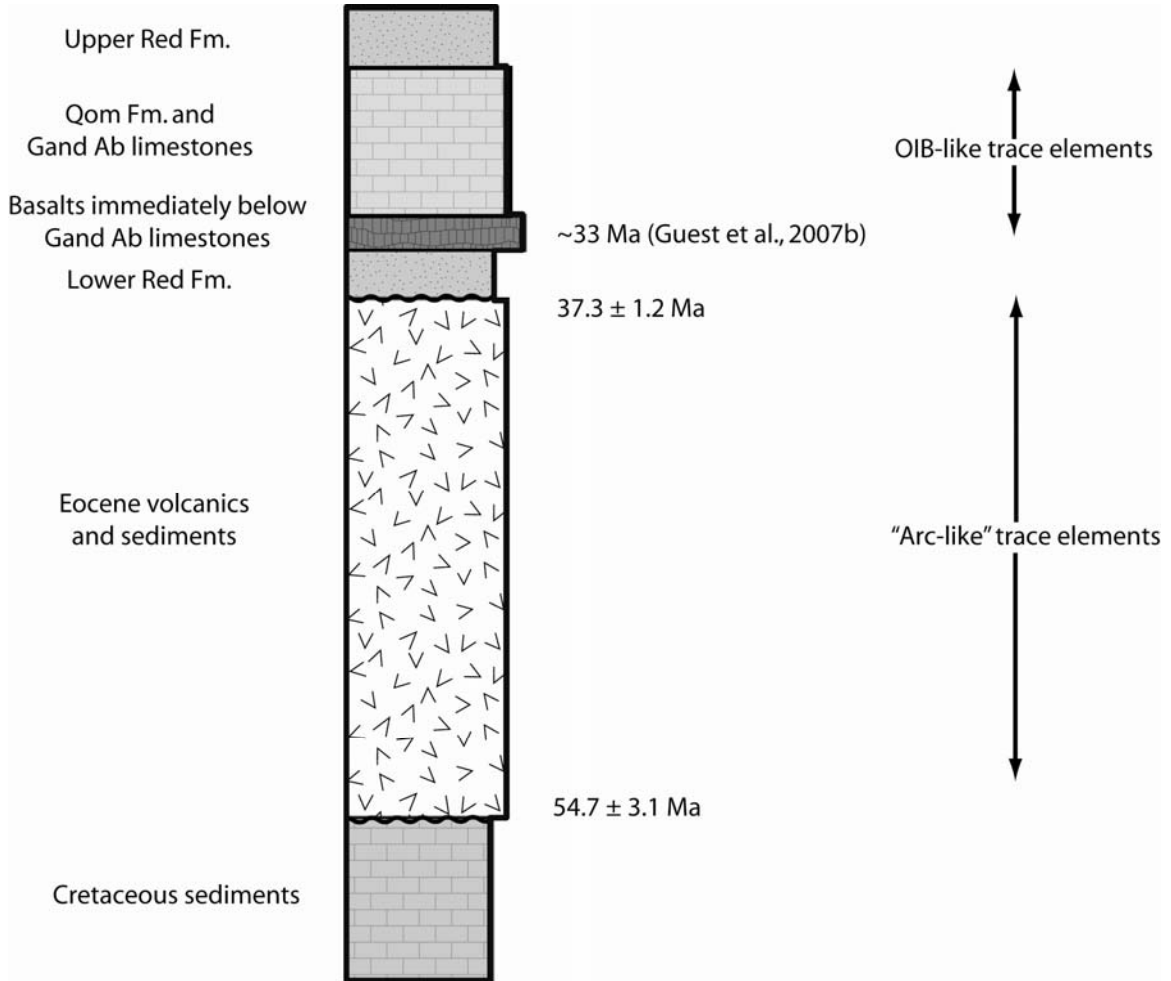


Figure 10



III-69

Figure 11

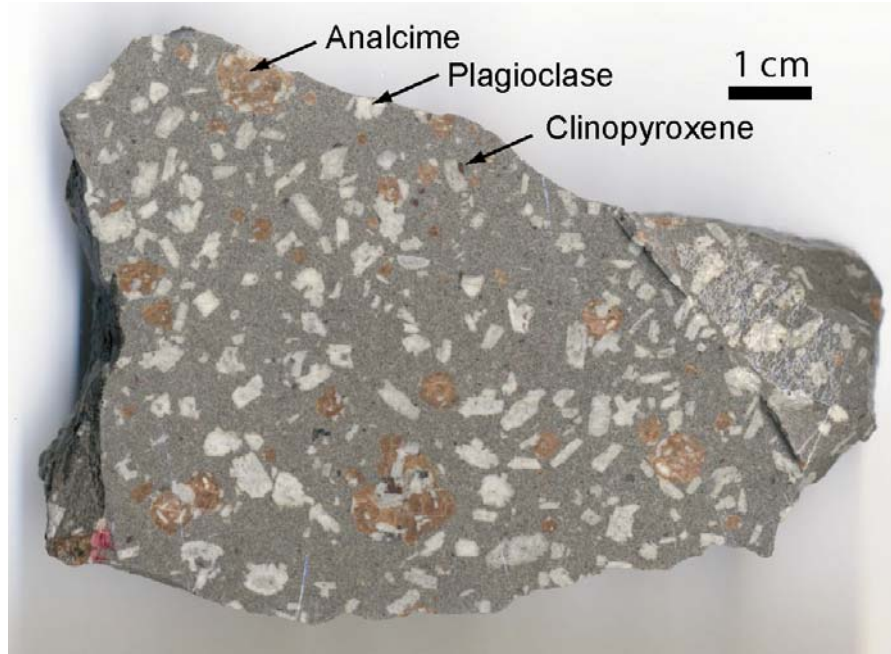


Figure 12

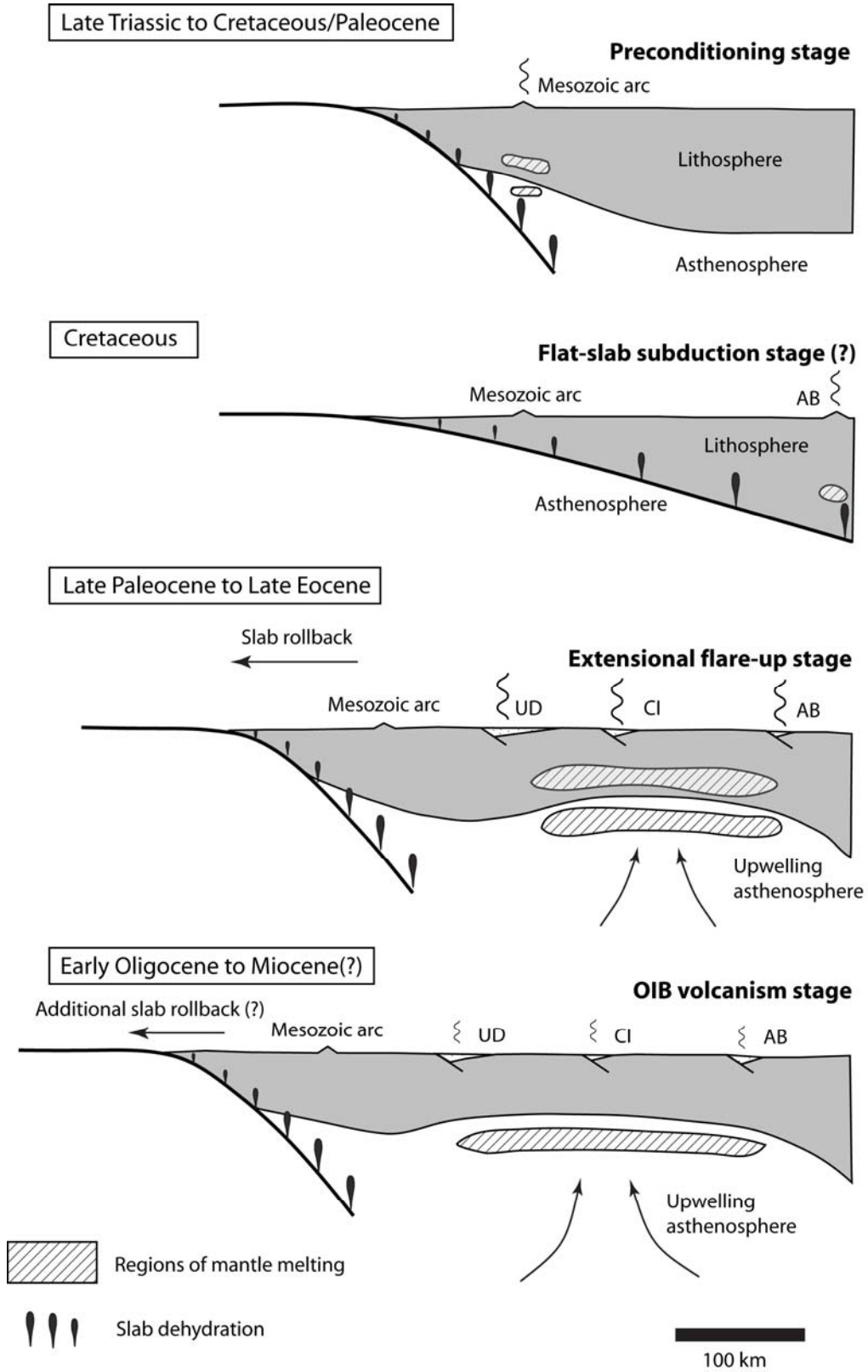


TABLE 1: U-Pb zircon age data

Sample/grain	Age (Ma) $^{206}\text{Pb}/^{238}\text{U}$	Age (Ma) $^{206}\text{Pb}/^{238}\text{U}$ 1 s.e.	Age (Ma) $^{207}\text{Pb}/^{235}\text{U}$	Age (Ma) $^{207}\text{Pb}/^{235}\text{U}$ 1 s.e.	$^{206}\text{Pb}^*/^{238}\text{U}$	$^{206}\text{Pb}^*/^{238}\text{U}$ 1 s.e.	$^{207}\text{Pb}^*/^{235}\text{U}$	$^{207}\text{Pb}^*/^{235}\text{U}$ 1 s.e.	Correlation of Concordia ellipses	UO/U	UO/U 1 s.e.
AB4_z1	42.13	2.71	40.22	4.81	0.00656	0.00042	0.04040	0.00493	0.6158	9.566	0.079
AB4_z2	41.57	2.36	37.49	3.92	0.00647	0.00037	0.03761	0.00401	0.5811	9.723	0.034
AB4_z3	39.33	2.95	7.63	33.60	0.00612	0.00046	0.00754	0.03330	0.4703	9.490	0.062
AB4_z4	41.61	2.58	42.34	3.90	0.00648	0.00040	0.04258	0.00401	0.6695	9.453	0.034
AB4_z5	42.53	2.44	42.37	2.57	0.00662	0.00038	0.04261	0.00264	0.9310	9.681	0.041
AB4_z6	40.88	2.37	35.83	3.28	0.00636	0.00037	0.03592	0.00335	0.6885	9.697	0.049
AB4_z7	41.12	2.35	43.54	3.31	0.00640	0.00037	0.04382	0.00340	0.7629	9.684	0.037
AB4_z8	39.62	2.22	35.80	3.38	0.00617	0.00035	0.03589	0.00345	0.6036	9.765	0.047
AB4_z9	40.84	2.51	39.08	6.00	0.00636	0.00039	0.03924	0.00615	0.5390	9.689	0.069
Ek5_z1	49.61	2.97	49.49	5.99	0.00773	0.00047	0.04995	0.00619	0.5246	8.086	0.062
Ek5_z2	46.20	3.36	39.96	9.51	0.00719	0.00053	0.04014	0.00974	0.4695	7.935	0.072
Ek5_z3	43.28	2.80	42.22	7.13	0.00674	0.00044	0.04246	0.00732	0.4878	8.172	0.071
Ek5_z4	46.49	2.70	51.16	5.20	0.00724	0.00042	0.05168	0.00539	0.6480	8.189	0.052
Ek5_z5	42.70	2.73	45.29	8.80	0.00665	0.00043	0.04561	0.00906	0.5404	8.178	0.069
Ek5_z6	44.48	2.90	49.98	18.44	0.00692	0.00045	0.05045	0.01910	0.4783	8.177	0.076
AB2_z1	45.44	3.30	23.26	47.82	0.00707	0.00052	0.02317	0.04820	0.5504	8.364	0.112
AB2_z2	52.86	3.62	46.04	22.32	0.00823	0.00057	0.04638	0.02300	0.4682	8.076	0.106
AB2_z3	47.39	3.45	29.60	21.55	0.00738	0.00054	0.02958	0.02180	0.4238	8.167	0.092
AB2_z4	50.37	2.95	39.96	7.31	0.00784	0.00046	0.04014	0.00748	0.4413	8.060	0.036
AB2_z5	50.52	3.28	49.78	17.05	0.00787	0.00051	0.05025	0.01760	0.4244	8.273	0.076
TR1_z1	56.56	2.81	59.79	5.30	0.00881	0.00044	0.06066	0.00554	0.1685	8.192	0.101
TR1_z2	49.72	2.14	56.60	5.98	0.00774	0.00034	0.05732	0.00622	0.4122	8.105	0.039

TABLE 1 (continued): U-Pb zircon age data

Sample/grain	Age (Ma) $^{206}\text{Pb}/^{238}\text{U}$	Age (Ma) $^{206}\text{Pb}/^{238}\text{U}$ 1 s.e.	Age (Ma) $^{207}\text{Pb}/^{235}\text{U}$	Age (Ma) $^{207}\text{Pb}/^{235}\text{U}$ 1 s.e.	$^{206}\text{Pb}^*/^{238}\text{U}$	$^{206}\text{Pb}^*/^{238}\text{U}$ 1 s.e.	$^{207}\text{Pb}^*/^{235}\text{U}$	$^{207}\text{Pb}^*/^{235}\text{U}$ 1 s.e.	Correlation of Concordia ellipses	UO/U	UO/U 1 s.e.
SA2_z1	40.12	1.75	77.70	5.29	0.00624	0.00027	0.07953	0.00562	0.6664	8.082	0.053
SA2_z2	49.23	3.03	232.90	33.10	0.00767	0.00047	0.25780	0.04100	0.8883	8.362	0.056
SA2_z3	36.11	1.55	48.07	4.45	0.00562	0.00024	0.04848	0.00460	0.3963	8.130	0.042
SA2_z4	38.91	2.05	53.73	4.17	0.00605	0.00032	0.05434	0.00433	0.4152	8.067	0.079
SA2_z5	39.29	1.95	44.12	3.96	0.00611	0.00031	0.04441	0.00408	0.5818	7.973	0.044
SA2_z6	36.34	1.62	40.75	2.97	0.00565	0.00025	0.04095	0.00304	0.6314	8.018	0.028
SA2_z7	37.40	1.82	48.36	4.84	0.00582	0.00028	0.04878	0.00500	0.4712	8.061	0.052
SA2_z8	39.34	1.63	58.25	5.35	0.00612	0.00025	0.05904	0.00558	0.5481	8.204	0.056
TF11_z1	44.89	3.19	43.98	6.19	0.00699	0.00050	0.04426	0.00637	0.5426	7.814	0.056
TF11_z2	48.13	3.13	49.39	5.42	0.00749	0.00049	0.04985	0.00560	0.6469	7.818	0.032
TF11_z3	44.07	2.66	39.54	6.77	0.00686	0.00042	0.03971	0.00693	0.4502	8.133	0.073
TF11_z4	46.17	2.91	41.75	8.21	0.00719	0.00046	0.04198	0.00843	0.4943	8.061	0.049
TF11_z5	43.01	2.51	39.92	4.53	0.00669	0.00039	0.04009	0.00464	0.6287	8.127	0.050
TF11_z6	41.54	2.49	37.81	5.55	0.00646	0.00039	0.03794	0.00568	0.4699	8.004	0.042
TF7A_z1	50.76	2.21	52.48	2.88	0.00791	0.00035	0.05304	0.00298	0.7204	7.995	0.018
TF7A_z2	47.06	2.41	82.04	6.45	0.00733	0.00038	0.08415	0.00689	0.6509	7.811	0.065
TF7A_z3	58.26	2.49	268.00	12.10	0.00908	0.00039	0.30200	0.01560	0.8331	8.174	0.033
TF7A_z4	49.53	2.09	62.27	5.16	0.00771	0.00033	0.06325	0.00541	0.4524	8.193	0.040
TF7A_z5	47.43	1.99	54.33	5.32	0.00739	0.00031	0.05497	0.00553	0.0726	8.285	0.105
TF7A_z6	48.44	2.29	61.59	4.64	0.00754	0.00036	0.06253	0.00486	0.5367	7.887	0.030
TF6_z1	52.77	2.36	55.43	3.24	0.00822	0.00037	0.05611	0.00337	0.7346	7.954	0.019
TF6_z2	53.40	2.41	57.01	4.30	0.00832	0.00038	0.05775	0.00447	0.7661	8.143	0.053

TABLE 1 (continued): U-Pb zircon age data

Sample/grain	Age (Ma) $^{206}\text{Pb}/^{238}\text{U}$	Age (Ma) $^{206}\text{Pb}/^{238}\text{U}$ 1 s.e.	Age (Ma) $^{207}\text{Pb}/^{235}\text{U}$	Age (Ma) $^{207}\text{Pb}/^{235}\text{U}$ 1 s.e.	$^{206}\text{Pb}^*/^{238}\text{U}$	$^{206}\text{Pb}^*/^{238}\text{U}$ 1 s.e.	$^{207}\text{Pb}^*/^{235}\text{U}$	$^{207}\text{Pb}^*/^{235}\text{U}$ 1 s.e.	Correlation of Concordia ellipses	UO/U	UO/U 1 s.e.
TF3_z1	49.31	3.25	54.54	13.28	0.00768	0.00051	0.05518	0.0138	0.4258	8.400	0.104
TF3_z2	55.54	4.25	73.49	42.19	0.00865	0.00066	0.07506	0.0447	0.5969	8.348	0.086
TF3_z3	57.48	3.74	51.92	11.84	0.00896	0.00059	0.05247	0.0123	0.4407	7.914	0.050
TF3_z4	56.40	4.04	57.21	15.35	0.00879	0.00063	0.05796	0.0160	0.4796	7.920	0.070
TF3_z5	54.29	3.87	61.87	12.51	0.00846	0.00061	0.06283	0.0131	0.4633	7.984	0.076
TF3_z6	57.71	4.24	61.84	13.62	0.00899	0.00066	0.06279	0.0143	0.5228	7.848	0.052

TABLE 2:  $^{40}\text{Ar}/^{39}\text{Ar}$  plagioclase age dataTF7A, plagioclase, 19.35 mg,  $J = 0.0019841 \pm 0.2384\%$ 

Step	T (°C)	t (min.)	$^{36}\text{Ar}$	$^{37}\text{Ar}$	$^{38}\text{Ar}$	$^{39}\text{Ar}$	$^{40}\text{Ar}$	% $^{40}\text{Ar}^*$	% $^{39}\text{Ar}$ rlsd	Ca/K	$^{40}\text{Ar}^*/^{39}\text{ArK}$	Age (Ma)	1 s.d.	
1	550	12	7.346	4.420	3.885	82.942	2972.64	28.8	24.3	0.45520565	10.350785	36.68	0.72	
2	580	12	1.689	5.754	1.224	52.422	1048.65	54.4	15.4	0.93773296	10.834842	38.37	0.43	
3	610	12	1.716	14.953	1.229	48.219	1037.62	53.4	14.1	2.65067641	11.450196	40.53	0.48	
4	640	12	1.649	26.719	0.907	34.55	884.597	47.9	10.1	6.618146	12.209336	43.18	0.58	
5	680	12	6.944	61.270	1.937	28.272	2466.82	19.6	8.3	18.6130145	17.226681	60.63	2.18	
6	730	12	5.969	105.38	1.923	21.502	2034.78	17.1	6.3	42.3919228	16.369872	57.66	1.96	
7	800	12	2.116	16.430	1.204	12.568	773.931	22.6	3.7	11.202965	13.797554	48.72	1.38	
8	890	12	1.485	2.802	0.947	7.484	545.841	23.0	2.2	3.20075722	16.431603	57.88	1.38	
9	1000	12	1.800	2.049	1.241	7.566	641.048	20.1	2.2	2.31461268	16.607316	58.49	1.85	
10	1140	12	3.146	1.928	3.120	13.428	1164.63	22.6	3.9	1.22675081	19.110076	67.14	1.70	
11	1290	12	4.454	1.509	5.580	26.394	1820.21	29.8	7.7	0.48836917	20.295339	71.22	1.41	
12	1400	12	3.873	1.061	4.020	5.874	1363.21	18.9	1.7	1.54341761	41.775679	143.66	4.62	
								Cumulative % $^{39}\text{Ar}$ released =	100.0			<b>Total gas age</b>	<b>48.55</b>	<b>0.48</b>

TABLE 2 (continued):  $^{40}\text{Ar}/^{39}\text{Ar}$  plagioclase age dataTF4A, plagioclase, 20.90 mg,  $J = 0.0020690 \pm 0.2015\%$ 

Step	T (°C)	t (min.)	$^{36}\text{Ar}$	$^{37}\text{Ar}$	$^{38}\text{Ar}$	$^{39}\text{Ar}$	$^{40}\text{Ar}$	% $^{40}\text{Ar}^*$	% $^{39}\text{Ar}$ rlsd	Ca/K	$^{40}\text{Ar}^*/^{39}\text{ArK}$	Age (Ma)	1 s.d.	
1	480	12	11.906	0.404	2.968	24.177	385.11	10.2	10.5	0.17313885	16.247516	59.65	6.42	
2	515	12	2.323	0.322	0.746	17.069	937.763	28.6	7.4	0.19546378	15.601342	57.31	2.02	
3	550	12	2.847	0.536	0.947	25.384	1214.62	32.3	11.1	0.2187894	15.408620	56.62	1.95	
4	585	12	4.030	1.040	1.221	27.736	1615.75	27.8	12.1	0.38853775	16.172201	59.38	2.37	
5	620	12	5.164	3.274	1.405	25.926	1882.15	20.5	11.3	1.30890186	14.879503	54.70	2.86	
6	655	12	2.041	5.066	0.687	16.486	832.02	29.6	7.2	3.18683073	14.817096	54.48	2.04	
7	700	12	8.878	1.764	2.029	13.5	2888.69	10.8	5.9	1.35436174	23.081534	84.16	8.78	
8	750	12	2.170	0.880	0.682	8.63	726.886	14.1	3.8	1.05682452	11.704218	43.17	3.27	
9	850	12	2.464	1.154	0.785	5.555	773.859	8.2	2.4	2.15375348	11.247561	41.50	4.95	
10	1000	12	3.421	1.471	1.214	8.205	1125.28	12.1	3.6	1.8585309	16.413969	60.25	5.34	
11	1200	12	8.894	2.817	4.621	18.294	2947.13	12.4	8.0	1.59617172	19.777279	72.35	6.36	
12	1400	12	34.04	4.149	14.142	38.287	11478.21	13.8	16.7	1.12313448	41.380797	148.20	11.19	
								Cumulative % $^{39}\text{Ar}$ released =	100.0			<b>Plateau age</b> <b>(steps 1-6)</b>	56.61	1.93
												<b>Isochron age</b> <b>(steps 2-7)</b>	50.90	2.20

note: isotope beams in mV, rlsd = released, error in age includes J error, all errors 1 sigma

 $^{36}\text{Ar}$  through  $^{40}\text{Ar}$  are measured beam intensities, corrected for decay for the age calculations

TABLE 3: Major and trace element compositions of Iranian Paleogene volcanic rocks

Sample	AN3	AN5	AR3	AR5	DV1	DV4	QM2	QM6	QZ2	SA5	SA7
Latitude (WGS84)	33.12397	33.13792	34.30428	34.31207	35.78198	35.73080	34.08575	34.87202	35.98157	36.22677	35.41140
Longitude (WGS84)	52.53003	52.54782	51.17087	51.23790	51.95788	51.87353	50.52168	49.90792	50.79127	50.58443	51.30395
Lithology	<i>Basaltic andesite</i>	<i>Andesite</i>	<i>Andesite</i>	<i>Trachy-basalt</i>	<i>Basalt</i>	<i>Basalt</i>	<i>Andesite</i>	<i>Basalt</i>	<i>Basalt</i>	<i>Basalt</i>	<i>Basalt</i>
SiO <sub>2</sub> (%)	53.02	59.27	59.31	46.87	47.38	49.07	58.04	48.56	46.65	50.00	49.49
TiO <sub>2</sub> (%)	1.09	1.10	1.32	1.73	0.42	1.04	0.97	1.42	1.97	1.09	1.04
Al <sub>2</sub> O <sub>3</sub> (%)	17.77	16.20	15.21	16.52	11.63	15.37	17.43	19.08	15.34	18.84	18.69
Fe <sub>2</sub> O <sub>3</sub> (%)	8.41	8.31	10.38	11.30	10.15	9.94	7.68	11.41	12.75	10.12	10.13
MnO (%)	0.15	0.15	0.21	0.26	0.19	0.17	0.12	0.20	0.20	0.17	0.17
MgO (%)	6.13	2.81	2.92	6.80	15.98	9.85	3.43	4.29	8.31	4.95	5.78
CaO (%)	8.42	5.48	3.72	10.49	12.75	10.43	7.84	9.93	10.20	10.06	10.13
Na <sub>2</sub> O (%)	3.46	3.78	3.72	3.11	0.85	1.76	3.00	3.98	3.25	2.80	2.71
K <sub>2</sub> O (%)	1.13	2.18	2.43	2.16	0.37	1.70	1.31	0.65	0.65	1.34	1.28
P <sub>2</sub> O <sub>5</sub> (%)	0.33	0.31	0.39	0.51	0.05	0.32	0.17	0.18	0.44	0.31	0.33
Total (%)	99.91	99.59	99.61	99.75	99.77	99.65	99.99	99.70	99.76	99.68	99.75
Nb (ppm)	14.6	9.2	11.3	46.7	1.0	4.9	2.4	8.6	14.5	7.0	6.0
Zr (ppm)	115	157	257	126	18	66	56	134	119	84	73
Y (ppm)	21.6	26.4	47.0	20.5	10.1	16.5	23.2	25.8	25.3	20.1	19.0
Sr (ppm)	426	444	190	866	424	552	365	220	878	642	699
U (ppm)	0	1	2	0	0	0	0	0	0	0	0
Rb (ppm)	17.5	62.8	68.4	51.1	10.2	35.5	14.2	36.7	8.4	30.2	26.0
Th (ppm)	2	10	8	3	1	3	1	5	2	2	2
Pb (ppm)	5	11	8	139	2	5	4	7	3	6	1
Ga (ppm)	17	17	17	16	11	15	22	18	17	18	18
Zn (ppm)	72	66	299	231	63	73	89	95	90	81	68
Ni (ppm)	84	4	1	50	296	131	10	6	86	17	23
Cr (ppm)	264	51	11	134	823	478	38	27	193	40	27
V (ppm)	160	151	148	188	147	226	276	186	225	224	209
Ce (ppm)	33	51	52	53	7	33	15	33	43	35	36
Ba (ppm)	363	496	651	1041	91	476	199	450	378	351	393
La (ppm)	14	22	21	26	3	18	2	15	19	14	13

TABLE 3 (continued): Major and trace element compositions of Iranian Paleogene volcanic rocks

Sample	SV4	TA1	TA3	TA5	DEHNAR1	MSHK1	TRD5	HSN1	NA3	7453
Latitude (WGS84)	35.26700	36.24017	36.23063	36.22677	34.30428	36.82298	35.47757	35.40928	32.22457	36.20155
Longitude (WGS84)	50.09178	50.58243	50.58340	50.58443	51.17087	58.12228	54.31718	51.30103	53.25290	51.00782
Lithology	<i>Basaltic trachy-andesite</i>	<i>Basalt</i>	<i>Basanite</i>	<i>Analcime phonotephrite</i>	<i>Basaltic andesite</i>	<i>Basalt</i>	<i>Analcime tephri-phonolite</i>	<i>Basalt</i>	<i>Analcime trachy-andesite</i>	<i>Basanite</i>
SiO <sub>2</sub> (%)	52.48	47.04	45.42	52.21	54.99	48.27	54.04	49.18	55.27	43.59
TiO <sub>2</sub> (%)	1.00	1.08	1.22	0.86	1.44	1.58	0.90	1.06	0.73	1.53
Al <sub>2</sub> O <sub>3</sub> (%)	17.22	16.57	14.22	19.64	16.36	17.13	17.74	19.06	20.66	15.46
Fe <sub>2</sub> O <sub>3</sub> (%)	8.04	10.46	12.23	7.91	9.38	9.56	7.51	10.10	5.77	10.74
MnO (%)	0.15	0.17	0.23	0.16	0.11	0.15	0.14	0.17	0.13	0.17
MgO (%)	7.28	8.95	7.29	2.75	1.62	8.02	2.37	5.30	1.79	8.48
CaO (%)	7.16	11.96	13.38	7.11	10.13	9.21	6.57	10.86	5.05	9.73
Na <sub>2</sub> O (%)	3.96	2.76	4.03	3.89	3.84	4.08	3.73	2.68	4.51	2.62
K <sub>2</sub> O (%)	1.87	0.60	1.36	4.64	1.56	0.93	6.08	1.24	5.24	1.29
P <sub>2</sub> O <sub>5</sub> (%)	0.47	0.36	0.50	0.78	0.33	0.57	0.60	0.28	0.56	0.68
Total (%)	99.63	99.95	99.88	99.95	99.76	99.50	99.68	99.93	99.71	94.29
Nb (ppm)	21.4	3.5	12.7	14.5	8.7	23.0	15.2	6.6	9.4	27
Zr (ppm)	201	36	114	158	200	199	202	73	157	142
Y (ppm)	21.1	17.1	25.4	21.5	36.1	22.5	18.8	18.4	20.0	23
Sr (ppm)	583	738	1247	1235	208	673	1410	646	932	775
U (ppm)	0	0	0	0	2	0	0	0	1	0.69
Rb (ppm)	37.9	12.0	125.2	165.4	46.5	13.4	126.5	26.3	189.6	20
Th (ppm)	7	2	11	14	6	3	12	2	12	2.2
Pb (ppm)	9	8	18	29	5	3	28	6	30	6
Ga (ppm)	16	15	16	17	17	17	19	17	17	NA
Zn (ppm)	70	63	100	69	166	75	70	80	72	108
Ni (ppm)	139	92	32	11	9	82	10	25	5	126
Cr (ppm)	242	230	70	39	63	174	22	50	10	189
V (ppm)	130	242	336	143	243	169	165	230	83	216
Ce (ppm)	59	27	112	87	40	58	82	30	57	71.2
Ba (ppm)	639	451	1402	1616	334	221	819	349	1362	431
La (ppm)	31	11	51	45	16	26	38	15	28	34.4